iScience

CellPress

Article

Dissecting N-Glycosylation Dynamics in Chinese Hamster Ovary Cells Fed-batch Cultures using Time Course Omics Analyses

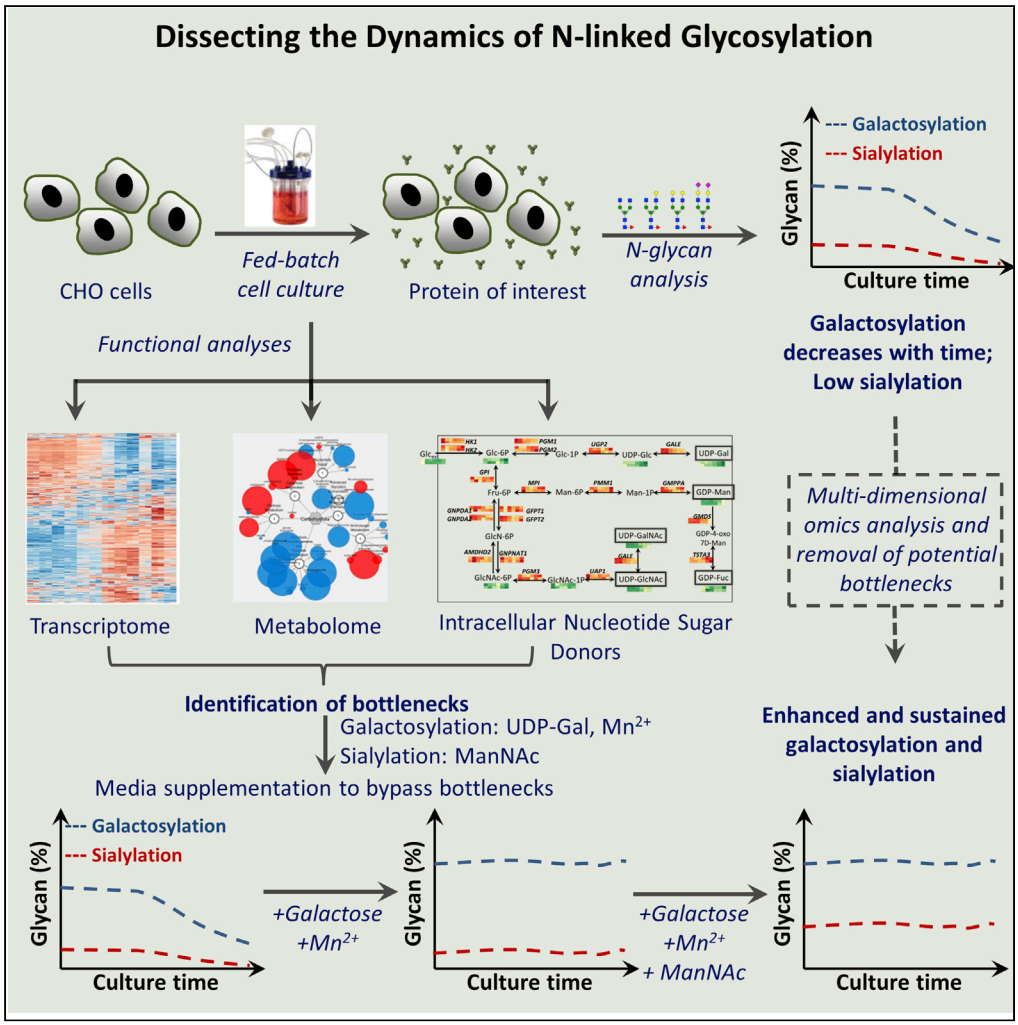

Madhuresh Sumit, Sepideh Dolatshahi, An-Hsiang Adam Chu, ..., Douglas A. Lauffenburger, Bhanu Chandra Mulukutla, Bruno Figueroa, Jr.

bhanuchandra.mulukutla@pfizer.com

HIGHLIGHTS

Major glycosylated species exhibit temporal dynamics during fed-batch processes

Key metabolic pathways linked to N-glycosylation exhibit significant temporal dynamics

Dynamics in nucleotide sugar donors (NSDs) directly influences glycoform heterogeneity

Glycoform heterogeneity can be mitigated by supplementing NSD biosynthetic precursors

Sumit et al., iScience 12, 102–120
February 22, 2019
https://doi.org/10.1016/j.isci.2019.01.006

iScience

CellPress

Article

Dissecting N-Glycosylation Dynamics in Chinese Hamster Ovary Cells Fed-batch Cultures using Time Course Omics Analyses

Madhuresh Sumit,[1] Sepideh Dolatshahi,[2] An-Hsiang Adam Chu,[3] Kaffa Cote,[3] John J. Scarcelli,[4] Jeffrey K. Marshall,[3] Richard J. Cornell,[3] Ron Weiss,[2] Douglas A. Lauffenburger,[2] Bhanu Chandra Mulukutla,[1,5,*] and Bruno Figueroa, Jr.[1]

SUMMARY

N-linked glycosylation affects the potency, safety, immunogenicity, and pharmacokinetic clearance of several therapeutic proteins including monoclonal antibodies. A robust control strategy is needed to dial in appropriate glycosylation profile during the course of cell culture processes accurately. However, N-glycosylation dynamics remains insufficiently understood owing to the lack of integrative analyses of factors that influence the dynamics, including sugar nucleotide donors, glycosyltransferases, and glycosidases. Here, an integrative approach involving multi-dimensional omics analyses was employed to dissect the temporal dynamics of glycoforms produced during fed-batch cultures of CHO cells. Several pathways including glycolysis, tricarboxylic citric acid cycle, and nucleotide biosynthesis exhibited temporal dynamics over the cell culture period. The steps involving galactose and sialic acid addition were determined as temporal bottlenecks. Our results show that galactose, and not manganese, is able to mitigate the temporal bottleneck, despite both being known effectors of galactosylation. Furthermore, sialylation is limited by the galactosylated precursors and autoregulation of cytidine monophosphate-sialic acid biosynthesis.

INTRODUCTION

Over the past decade, monoclonal antibody (mAb) therapeutics has shown significant success in clinical studies and constitutes the majority of biologically derived drugs (Niwa and Satoh, 2015; Sha et al., 2016). More than 30% of the new drugs licensed currently are based on mAbs and biological therapeutics (Niwa and Satoh, 2015; Sathish et al., 2013). N-linked glycosylation (N-glycosylation) is known to play a key role in governing the potency, safety, immunogenicity, and pharmacokinetic clearance of these proteins. It can therefore be a critical quality attribute of such biologically derived therapeutic proteins (Berger et al., 2011; Eon-Duval et al., 2012; Maverakis et al., 2015). N-glycosylation is a complex network of reactions resulting in a number of possible glycoform structures (Hossler et al., 2006; Krambeck and Betenbaugh, 2005). As a result, despite consistent protein backbones, a number of different glycosylation isoforms (glycoforms) are observed on recombinant proteins purified from the harvest of a Chinese hamster ovary (CHO) cells fed-batch process. Therefore, a robust control strategy is needed during the course of a culture to dial in a desired harvest glycosylation profile accurately.

Glycoform produced at any given time point in a cell culture process is heterogeneous. For example, there could be 5% mAbs with high mannose species, another 25% mAbs with galactosylated species, etc. (Figure 1A). However, this heterogeneity in glycoform also changes with time, or exhibits temporal dynamics. Both of these contribute toward the heterogeneity in glycoform observed at the harvest, also called cumulative glycoform. We hypothesize that the temporal variation in glycoform distribution is likely due to the kinetics of the metabolic components in the glycosylation network during CHO fed-batch cultures. Such temporal dynamics in glycosylation network activity can be due to changes in factors including sugar nucleotide levels, glycosylation enzyme levels, and availability of cofactors such as metal ions. These factors are, in turn, influenced by changes in cell culture process parameters including, but not limited to, culture nutrient levels (Fan et al., 2015), pH (Lin et al., 2015; Villiger et al., 2016a), levels of by-products such as lactate and ammonia (Fan et al., 2015; Gawlitzek et al., 2000), and temperature (Ivarsson et al., 2014; Sou et al., 2015). Several groups have developed mathematical models to probe the heterogeneity of glycoforms in a cell culture process (Hossler et al., 2007; Jedrzejewski et al., 2014; Jimenez del Val et al., 2011;

[1]Culture Process Development, Bio Therapeutics Pharmaceutical Sciences, Pfizer, 1 Burtt Road, Andover, MA 01810, USA

[2]Department of Biological Engineering, Massachusetts Institute of Technology, Cambridge, MA 02139, USA

[3]Analytical Research and Development, Bio Therapeutics Pharmaceutical Sciences, Pfizer, 1 Burtt Road, Andover, MA 01810, USA

[4]Cell Line Development, Bio Therapeutics Pharmaceutical Sciences, Pfizer, 1 Burtt Road, Andover, MA 01810, USA

[5]Lead Contact

*Correspondence: bhanuchandra.mulukutla@pfizer.com

https://doi.org/10.1016/j.isci.2019.01.006

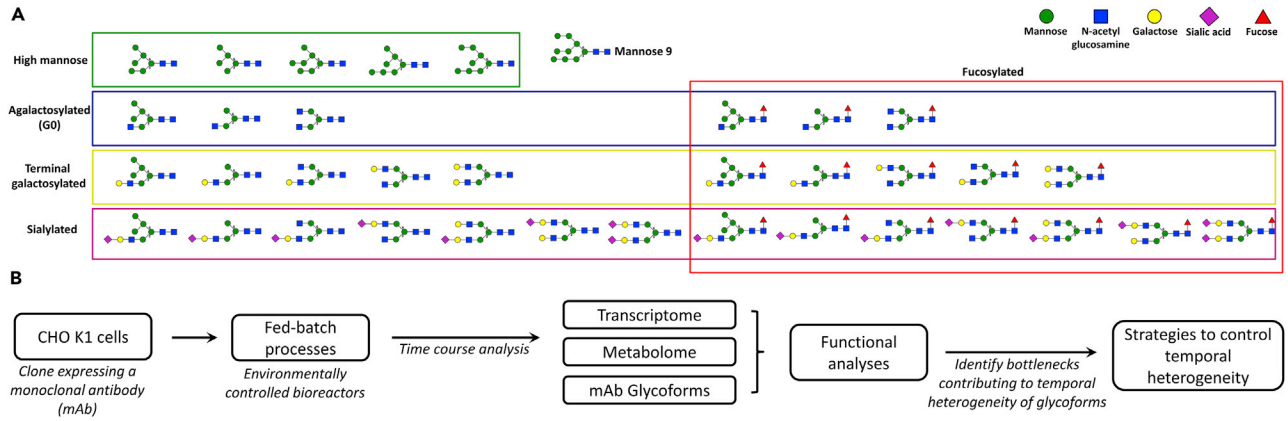

Figure 1. Schematic of the Study

(A) Glycoform heterogeneity in the monoclonal antibodies observed in the harvest of a fed-batch culture.

(B) Clonally propagated CHO-K1 cells with random integration of a monoclonal antibody gene were grown under two different processes, and time course analysis was performed on the transcriptome, metabolome, and mAb glycoform data to identify key bottlenecks.

Jiménez del Val et al., 2013; Kaveh et al., 2013; Krambeck et al., 2009; Villiger et al., 2016b). Only recently, with the availability CHO genome data (Lewis et al., 2013), several groups have implemented time course omics analysis of CHO fed-batch cultures to probe the system as a whole (Hsu et al., 2017; Mulukutla et al., 2012; Opdam et al., 2017; Sha et al., 2018). However, our understanding of the dynamics in the intracellular factors influencing N-glycosylation, including levels of nucleotide sugar donors (NSDs), glycosyltransferases, and glycosidases, remains insufficient owing to the lack of an integrative and quantitative analyses of the same. In this study, a systems approach that employs multi-prong omics analyses was used to probe the glycosylation physiology of CHO cells in fed-batch cultures with the specific goal of dissecting the temporal dynamics in NSD synthesis, glycosylation-related gene expression, and levels of cofactors that play a key role in the glycosylation reaction network.

Briefly, in this study, a CHO-K1-derived cell line expressing a model mAb was cultivated in environmentally controlled bioreactors using two distinct fed-batch processes (Figure 1B). Time course transcriptomics (RNA sequencing [RNA-seq] analysis), metabolomics, and glycan analyses were performed on the two processes. Statistical and functional analyses, including principal-component analysis (PCA), gene set enrichment analysis (GSEA) (Subramanian et al., 2005), time course gene set analyses (TCGSA) (Hejblum et al., 2015), and time course differential gene and metabolite expression analyses (maSigPro) (Conesa et al., 2006), were performed on the omics data to identify pathways that were differentially regulated between the two processes or, within a process as a function of time. This helped identify potential factors that could be responsible for temporal dynamics in glycosylation reaction kinetics. Additional experiments were performed to validate and confirm the role of these factors in temporal dynamics of glycosylation.

RESULTS

Major Glycosylated Species Show Similar Temporal Dynamics across the Two Fed-Batch Processes Employed but Vary in Their Absolute Values

A CHO-K1 host-cell-derived clone producing a model mAb was cultivated in two distinct 12-day fed-batch cell culture processes, namely, platform (CC) and HiPDOG (HD), carried out in 1-L working volume bioreactors (see the Transparent Methods for details on the process differences between CC and HD). Higher peak cell densities and titers were observed in the HD process than those observed in the CC process (Figure 2A). Peak lactate levels were significantly lower in the HD (~2 g/L) than in the CC process (~4 g/L). However, cells in CC culture underwent a strong metabolic shift to lactate consumption on day 5 of the process. The higher viable cell density observed in the HD process could therefore be due to the relatively lower peak lactate levels when compared with the CC process. Specific productivity or the amount of protein produced per cell per day (q_P) was similar across both processes and increased over time until day 9 (Figure 2A). The dynamics of other process-related parameters and extracellular metabolites is shown in Figure S1A.

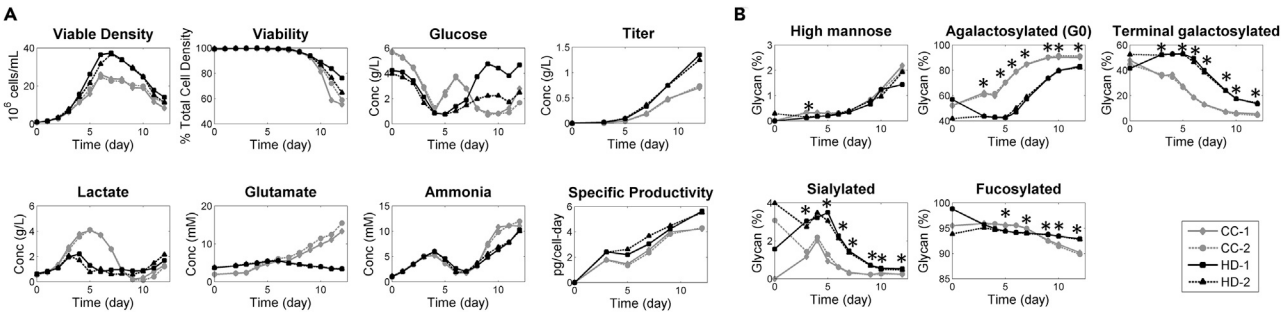

Figure 2. Glycan Species from the mAbs Exhibit Similar Time Dynamics Despite Process Variation

(A) The two processes resulted in widely varying lactate profiles as well as cell growth and titer.

(B) Agalactosylated (G0) and high-mannose species increase over time, whereas terminal galactosylated and sialylated species decrease over time. Slight decrease in fucosylated species is also observed over time. A detailed classification of the glycan structures is provided in Data S2. Asterisks (*) represent $p < 0.05$ for two-tailed unpaired t tests comparing CC and HD samples from each day.

Hydrophilic interaction chromatography-based glycan analysis was performed on the mAb molecules present in the spent media samples collected from different days of the two processes across the exponential "growth phase" (days 0, 3, 5) and the stationary "production phase" (days 7, 9, and 12) (Data S1). These glycan structures were then classified into major glycosylated species (Data S2). Each major glycosylated species had similar temporal dynamic patterns in both processes, but differed in the absolute level of the species measured (Figures 2B and S1B). For example, the levels of high mannose species, which is primarily the glycan core with five or more mannose moieties, and the agalactosylated species (G0) increased over time in both processes. However, terminally galactosylated species (term-gal) that have either one (G1) or two (G2) galactoses terminating the glycan chain decreased significantly over time across both processes. Furthermore, a slight decrease in the sialylated and fucosylated species was also observed over time in both processes. To understand the glycan profile of the mAbs at specific time points during the culture, instantaneous glycan profiles were calculated by taking the time derivative of the cumulative glycans with respect to the titer produced (Figure S1C, see Transparent Methods). These results suggested that there are two observations that needed explanation, namely, the absolute differences in the levels of major species (specifically galactosylation/agalactosylation) between the two fed-batch processes and the temporal changes in the major glycan species (which are relatively conserved across the two processes).

To explain the absolute differences in the major species between the two processes, differences in the spent culture media for the two processes were probed. As the two processes were implemented in distinct basal and feed media, a detailed metal ion analysis was performed to understand the differences between the processes (Figure S1D). Manganese, a known cofactor (Witsell et al., 1990) for the enzyme beta-1,4-galactosyltransferase-1 (*B4GALT1*), which catalyzes the addition of galactose to the extending glycan chain, was observed to be significantly lower in the CC samples. Although other metal ions such as Mg^{2+}, Ca^{2+}, and Cu^{2+} also showed differences between the two fed-batch processes and they could be potential covariates in contributing to the absolute differences, the goal was to identify the major influencing factor. As Mn^{2+} is directly linked to the galactosylation step, we hypothesized that manganese level could be the main reason for the differences in the absolute levels of term-gal species between the two processes. To test this, a fed-batch experiment was conducted in shake flasks with pH adjustment, by inoculating cells in the two basal media but with the manganese levels swapped between them (Figure S1E). Cells were inoculated in original or modified versions of CC and HD media. Modified versions of each medium had Mn^{2+} levels adjusted to match the starting levels in the original formulation of the other medium. This experiment was part of a bigger experiment described later in the last subsection of the Results section. The absolute levels of term-gal produced in the two media were found significantly different and corresponded to the swapped manganese concentrations. This established that the absolute difference in the galactosylated (and agalactosylated) species was mainly due to the difference in the culture manganese levels between the two processes.

From the instantaneous glycan profiles, it was apparent that throughout the fed-batch process, most of the glycans produced have the mannose sugars trimmed and N-acetylglucosamine (GlcNAc) added to them (Figure S1C). However, the amount of agalactosylated species increased with time, whereas those of the

galactosylated and sialylated species decreased over time. This suggested that the conversion of high-mannose species into low-mannose species and the subsequent addition of GlcNAc in the Golgi might not have bottlenecks, but the steps involving galactosyl and sialyl transfer might be rate-limiting steps in the glycosylation reaction network. The reaction steps involving glycan chain extension in the N-glycosylation process are highly ordered and sequential. Under pseudo-steady-state assumption, the turnover rate (which includes factors such as precursor, substrate, enzyme concentrations and enzyme activity influenced by enzymatic rate constants, as well as steric hindrance) of reactants to products governs the fraction of substrate converted into product. For successive reaction steps, under no rate limitation, one can plot the substrate and product levels on x and y axes, respectively. For example, if all the glycans attached to mAbs exist as the terminal species, i.e., completely sialylated species, on a scatterplot of n^{th} species as y axis and $(n-1)^{th}$ species as x axis, the data should fall on the y axis, i.e., $(n-1)^{th}$ species ~0% and n^{th} species ~100%. For the rest of the intermediate species, because their levels are near zero, on a scatterplot of i^{th} (y axis) and $(i-1)^{th}$ species (x axis), the data should fall at the intersection of the x and y axes, i.e., $(i-1)^{th}$ species ~0% and i^{th} species ~0%. Alternatively, under rate limitation scenario, the scatterplot would be shifted to non-zero values due to significant buildup of the intermediate species, as seen in case of several glycosylated species (Figure S2). This alternative approach using quasi-steady-state analysis of instantaneous glycan profiles supports the same conclusion that the steps involving galactosyl and sialyl transfer might be rate-limiting steps in the glycosylation reaction network (Figure S2). Temporal variation observed in the glycoforms produced could be an outcome of these bottlenecks in the galactosylation and sialylation steps. To investigate the other potential reasons for the dynamic nature of the glycosylation profile, and to identify the bottlenecks in the galactosylation and sialylation steps, systems analysis approach integrating transcriptomic and metabolomic data was undertaken.

Systems Analysis Suggests that CHO Cells Undergo a Shift in Their Transcriptional, Metabolic, and Glycome Program along the Course of a Fed-Batch Culture

Time course analyses of global transcript levels (RNA-seq) as well as intra- and extracellular metabolite levels were performed for the samples collected from both CC and HD processes (see the Transparent Methods and Data S3, S4, and S5). Pairwise clustering, using the Spearman correlation was used to cluster samples based on the transcriptional profile of the genes constituting the top 10% variance (Figure 3A [i]). Irrespective of the process employed, the samples within each phase, i.e., growth or production phase, clustered together. Next, pairwise clustering was performed on the time course extracellular and intracellular metabolomic data (Figure 3A [ii, iii]). Similar to the transcriptomic data, the metabolomics data also showed clustering of samples based on growth or production phase, irrespective of the processes. Alternatively, PCA performed on the transcriptome data showed that the trajectory of change in the variance over the course of the culture, as explained by principal component 1 (PC1) and PC2 or PC3, appears to be primarily dictated by the growth or production phase of the culture, together explaining 75% of the total variance (Figure 3B [i]). PCA of the metabolomics data revealed similar shift in the metabolic state of the cells during the growth and production phases, together explaining 63% and 52% of the variance for the extracellular and intracellular metabolites, respectively (Figure 3B [ii, iii]). These analyses showed that the metabolic and transcriptional footprints of samples correlated well within growth or production phase, despite different processes being employed.

Similar clustering analysis of the standardized (*Z* scored) glycan data for the time course samples suggested that the glycan profiles also appeared to be dependent on the stage of the culture (Figure 3A [iv]). Interestingly, HD1D7 and HD2D7 samples from HD process clustered with growth phase (days 0, 3, 5). Glycan addition to the mAbs is downstream of all the steps, including transcription, translation, and metabolism (nucleotide synthesis). Therefore, a time delay (or lag) is possible, explaining why HD1D7 and HD2D7 glycoforms cluster with growth phase rather than the production phase. In addition, PCA analysis was performed on a list of glycosylation-related genes curated from the literature (Nairn et al., 2008). Only those genes that were expressed at least for one time point for both the processes were considered in the analysis (Data S6). Similar to the clustering analysis, variance in the glycan-related genes was a function of the state of cells and appeared to be independent of the process (Figure 3B [iv]). Next, correlation analysis was performed on the process parameter data from different days of the two processes, spanning growth and production phases (see Figure 3 legends). Interestingly, unlike the transcriptome and metabolome, the process parameters clustered together based on the process employed (CC or HD) (Figure 3C). Together, the results suggested that although the cells are subjected to relatively different process conditions, the transcriptome, metabolome, and to an extent the N-glycan signature seemed to be dictated primarily by the culture

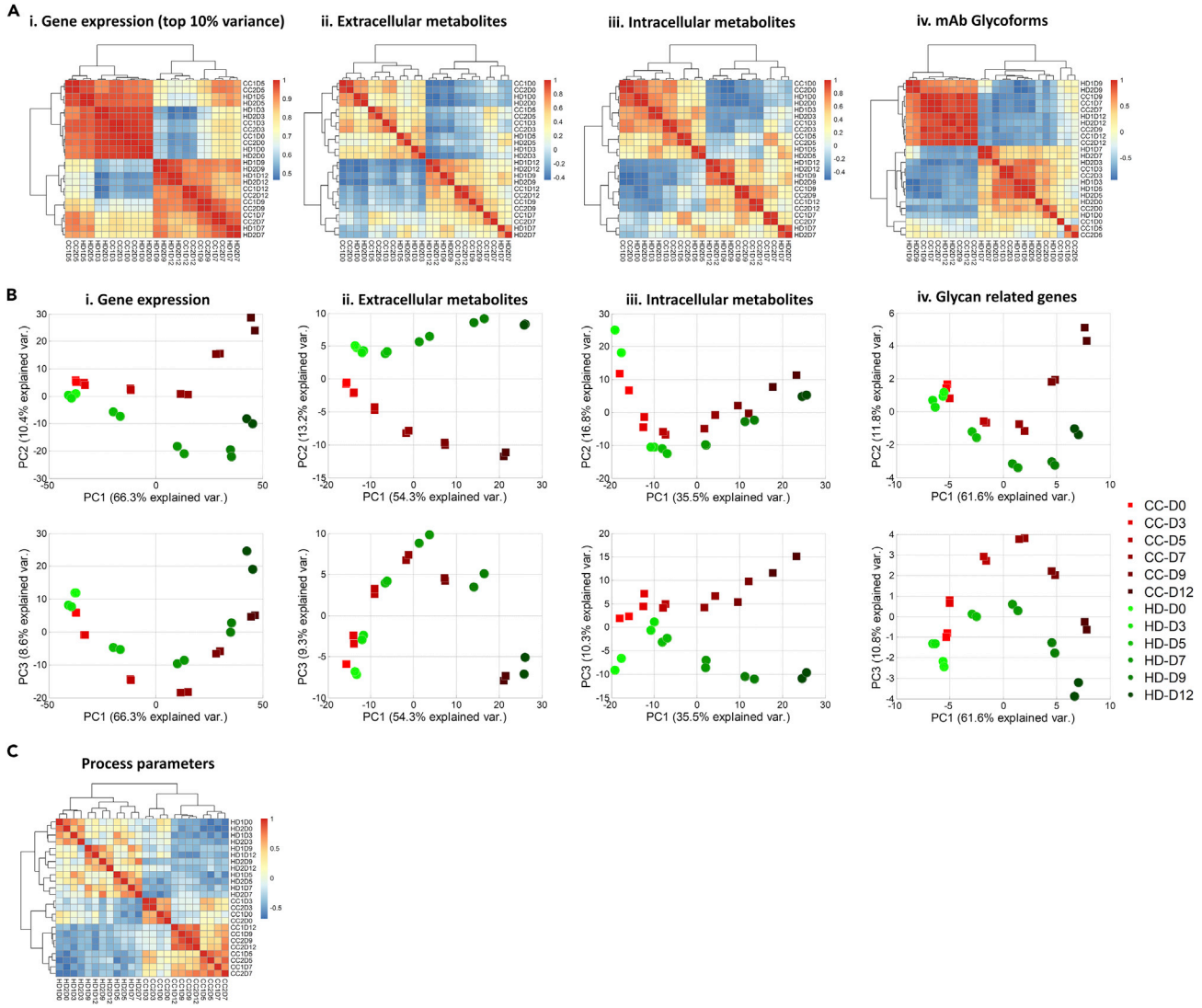

Figure 3. CHO Cells Undergo a Shift in Transcriptional and Metabolic Profile during Cell Culture

(A) Time course data for (i) genes that constitute top 10% variance across the samples, (ii) the intracellular metabolites, (iii) extracellular metabolites, and (iv) mAb glycoforms were correlated with all other samples, and the samples were clustered based on their pairwise Spearman correlation coefficients.

(B) Principal-component analysis of the transcriptomic, metabolomic, and glycan data. The first and second (top panel) or third (bottom panel) principal components together account for ~60%–90% of the variance in the omics data and show temporal shift in the CHO transcriptional and metabolic profile from growth phase (day 0 to day 7) to production phase (day 7 to day 12).

(C) Time course data for process parameters were correlated with all other samples, and the samples were clustered based on their pairwise Spearman correlation coefficients showing that the parameters cluster separately for the two process conditions (HD and CD), regardless of the growth phase and production phase. Process variables included in the analysis are glucose, lactate, glutamate, pH, media feed, base feed, glucose feed, and ICP metals (fed differently in the two processes). As the units of each of the variables differ, the data were z-normalized for each variable before calculating the Spearman correlations.

stages (growth or production phase). These results motivated a detailed functional analysis of the time course omics data to gain insights into the complex regulation of N-glycosylation dynamics.

Functional Analysis of the Omics Data Identified Significant Time Dynamics in Key Metabolic Pathways Linked to N-Glycosylation

An integrative approach, employing three orthogonal methods, was taken to analyze the multi-dimensional omics data. These methods include GSEA, TCGSA, time course metabolite set analysis (TCMSA), and maSigPro. GSEA was employed to identify functional classes that are enriched in either the growth

phase or the production phase of the culture. TCGSA or TCMSA were used to capture the functional classes (gene sets or metabolic sets) that may or may not have dynamics in one phase or the other, but might show dynamics over the course of the complete culture. maSigPro was used to identify key genes or metabolites that exhibit significant temporal dynamics (i.e., the genes and metabolites that were significantly perturbed over time) using a regression-based analysis (see Transparent Methods). The analyses were performed on data from both processes separately, and unless otherwise stated, the results/trends from these analyses hold true for both processes.

For GSEA and TCGSA functional class analyses, a composite curated gene set list was used comprising gene sets from KEGG, BioCarta, Reactome, and additional gene sets related to glycosylation from Gene Ontology (Data S7, see also Transparent Methods). Employing GSEA, several pathways were found to be enriched in the growth phase including central energy metabolism, cell cycle, apoptosis, and protein synthesis (Data S8A and S8B, Figure S3). In contrast, several other pathways including those involved in glycosylation, aminoglycan metabolism, glycerolipid metabolism, sphingolipid metabolism, and cell adhesion were enriched in the production phase. TCGSA analysis identifies the gene sets that exhibit time dynamics over the complete duration of the culture irrespective of the changes in the growth or production phases of the culture (see methods section in Transparent Methods for more details). Employing TCGSA and using the same gene set list that was used for GSEA, gene sets such as those related to NSD biosynthetic pathways, pentose phosphate pathway, and oxidative phosphorylation, among others, were identified to have time dynamics over the complete time span of the culture. Interestingly, these gene sets were not enriched in GSEA (Data S9).

Apart from transcription level control of enzyme/metabolic pathway activity, it is well known that changes in metabolic pathway flux can also be influenced significantly by intermediate metabolite levels (Hackett et al., 2016; Mulukutla et al., 2016). To investigate temporal changes in metabolite levels across the fed-batch processes, TCMSA was performed on the intracellular metabolomic dataset. A curated list of metabolites based on their functional classes was employed for the analysis (Data S10). The analysis suggested that several pathways that exhibit significant temporal dynamics at the transcriptional level also vary significantly at the metabolite level. These include sphingolipid metabolism, fatty acid metabolism, purine and pyrimidine metabolism, nucleotide sugar metabolism, amino acid metabolism, and glycolytic pathway (Data S11). In addition, a statistical test (maSigPro) was employed to identify key transcripts and metabolites that show significant time dynamics. Top transcripts and intracellular metabolites that vary significantly over time were ranked based on their q-values for the maSigPro test, and a ranked list is shown for overall data as well as for various functional groups (Data S12) and metabolic pathways (Data S13).

Combining the results from all the functional set and statistical analyses, a list of key pathways that exhibit significant time dynamics in CHO cells during fed-batch culture time course was curated (Table 1). For each functional class listed in the table, gene/metabolites that had significant time dynamics are also included. Several pathways from this list were identified as potential regulators of N-glycosylation dynamics because of their direct or indirect linkage with the N-glycosylation process (Figure 4). Next, temporal changes in these specific pathways were explored.

Temporal Dynamics in Levels of Enzyme Transcripts and Intermediate Metabolites of Metabolic Pathways Influencing N-Glycosylation Dynamics

Glycolysis

The glycolytic pathway was found to be enriched in the growth phase (GSEA). TCGSA suggested that glycolytic gene sets exhibit significant temporal perturbation or dynamics (Table 1). Glycolytic metabolites such as glucose-6-phosphate (G6P) and fructose-6-phosphate (F6P) serve as precursors to the NSD biosynthetic pathways. Therefore, changes in the transcript levels of glycolytic enzymes and in the corresponding metabolites can potentially influence the flux directed toward NSD biosynthesis. Glucose consumption rates (qGlc) and lactate production rates (qLac) have been used as indicators of the dynamics in central energy metabolism. For both processes, the metabolic state of the cells in the bioreactors shifted from lactate-producing (qLac/qGlc>0) to lactate-consuming state (qLac/qGlc<0) and again to a marginally lactate-producing state toward the end of the culture (Figure S4A). Such metabolic shifts are known to be outcomes of changes in the glycolytic gene expression and intermediate metabolite levels (Hartley et al., 2018; Mulukutla et al., 2012). Several glycolytic enzymes, including ADP-dependent glucokinase (*ADPGK*), 6-phosphofructo-2-kinase (*PFKFB4*), triosephosphate isomerase (*TPI*), hexokinase-2 (*HK2*), and

Pathway/ Functional Sets (GSEA Enrichment Phase)	Significant Gene Sets (GSEA and TCGSA)	Significant Metabolic Sets (TCMSA)	Top Significant Genes (maSigPro)	Top Significant Metabolites (maSigPro)
Sphingolipid metabolism (production phase)	REACTOME_SPHINGOLIPID_METABOLISM REACTOME_GLYCOSPHINGOLIPID_METABOLISM KEGG_GLYCOSPHINGOLIPID_BIOSYNTHESIS_GANGLIO_SERIES KEGG_SPHINGOLIPID_METABOLISM REACTOME_SPHINGOLIPID_DE_NOVO_BIOSYNTHESIS	Sphingolipid metabolism	ASAH1 SMPD1 PSAP GM2A	Glycosyl-N-nervonoyl-sphingadienine N-nervonoyl-sphingadiene N-erucoyl-sphingosine sphingomyelin
Cell adhesion &extracellular matrix (production phase)	KEGG_CELL_ADHESION_MOLECULES_CAMS KEGG_ECM_RECEPTOR_INTERACTION REACTOME_COLLAGEN_FORMATION REACTOME_EXTRACELLULAR_MATRIX_ORGANIZATION REACTOME_DEGRADATION_OF_THE_EXTRACELLULAR_MATRIX	NA	NEO ICAM1 SDC1 PTPRM	NA
Amino acid metabolism (growth phase)	REACTOME_METABOLISM_OF_AMINO_ACIDS_AND_DERIVATIVES[a] REACTOME_AMINO_ACID_AND_OLIGOPEPTIDE_SLC_TRANSPORTERS[a]	Lysine and histidine metabolism Urea cycle, arginine, and proline metabolism Gammaglutamyl amino acid Tyrosine and phenylalanine metabolism Tryptophan metabolism	SMS AHCY SLC25A15 CBS GOT1	Taurine Pipecolate Argininate N-acxetylhistidinemethionine sulfoxide
Phospholipid metabolism (production phase)	REACTOME_GLYCEROPHOSPHOLIPID_BIOSYNTHESIS REACTOME_PHOSPHOLIPID_METABOLISM KEGG_GLYCEROPHOSPHOLIPID_METABOLISM	Phosphatidylglycerol/phosphatidylinositol Phosphatidylcholine Lysophospholipid	PNPLA2 PNPLA8 PCYT1A DGAT2 PLD3	CDP-ethanolamine 1,2-dioleoyl-GPG 1-palmitoleoyl-2-oleoyl-glycerophosphoglycerol 1-palmitoyl-2-stearoyl-glycerophosphocholine 1,2-dipalmitoleoyl-glycerophosphocholine
Amino sugar and NSD metabolism (NA)	KEGG_AMINO_SUGAR_AND_NUCLEOTIDE_SUGAR_METABOLISM[a] GO_NUCLEOTIDE_SUGAR_BIOSYNTHETIC_PROCESS[a]	Amino sugar and nucleotide sugar	GALE UGDH FPGT PGM2 GMDS	Glucuronate UDP-galactose UDP-glucose UDP-GlcNAc/UDP-GalNAc CMP-N-acetylneuraminic acid
Pyrimidine metabolism (growth phase)	GO_PYRIMIDINE_NUCLEOTIDE_BIOSYNTHETIC_PROCESS GO_PYRIMIDINE_NUCLEOTIDE_METABOLIC_PROCESS KEGG_PYRIMIDINE_METABOLISM REACTOME_PYRIMIDINE_METABOLISM	Pyrimidine metabolism Pyrimidine metabolism uracil containing	PRPS1 TYMS UNG DUT TDG	Thymidine 2′-O-methylcytidine 5-methylcytidine 5-methyl-2′-deoxycytidine beta-alanine

Table 1. Key Functional Groups and Pathways that Exhibit Significant Temporal Dynamics over the Cell Culture Period during Fed-Batch Processes

(Continued on next page)

Pathway/ Functional Sets (GSEA Enrichment Phase)	Significant Gene Sets (GSEA and TCGSA)	Significant Metabolic Sets (TCMSA)	Top Significant Genes (maSigPro)	Top Significant Metabolites (maSigPro)
Purine metabolism (growth phase)	REACTOME_PURINE_RIBONUCLEOSIDE_ MONOPHOSPHATE KEGG_PURINE_METABOLISM REACTOME_PURINE_METABOLISM	Purine metabolism	RRM2 IMPDH2 RRM1	N1-methylinosine N2,N2-dimethylguanosine 7-methylguanine
Cell cycle, mitosis, and apoptosis (growth phase)	KEGG_CELL_CYCLE REACTOME_CELL_CYCLE REACTOME_CELL_CYCLE_CHECKPOINTS REACTOME_CELL_CYCLE_MITOTIC REACTOME_REGULATION_OF_APOPTOSIS	NA	LMNB1 ZWILCH POLE CDC6	NA
Glycosylation (production phase)	GO_GLYCOSYLATION GO_N_GLYCAN_PROCESSING GO_PROTEIN_N_LINKED_GLYCOSYLATION REACTOME_N_GLYCAN_TRIMMING_IN_THE_ER	NA	MAN1B1 DDOST ALG13 B4GALT1	NA
Amino glycans (production phase)	KEGG_GLYCOSAMINOGLYCAN_DEGRADATION REACTOME_GLYCOSAMINOGLYCAN_METABOLISM KEGG_GLYCOSAMINOGLYCAN_BIOSYNTHESIS_	NA	GNS CHPF HMMR	NA
TCA cycle (growth phase)	MOOTHA_TCA KEGG_CITRATE_CYCLE_TCA_CYCLE REACTOME_CITRIC_ACID_CYCLE_TCA_CYCLE REACTOME_METABOLISM_OF_CARBOHYDRATES	TCA cycle	FH ACLY ME1 SDHC SDHB	Malate Aconitate Citrate Succinate 2-methylcitrate/homocitrate
Glycolysis and gluconeogenesis (growth phase)	REACTOME_GLUCOSE_TRANSPORT REACTOME_REGULATION_OF_GLUCOKINASE REACTOME_GLUCONEOGENESIS BIOCARTA_GLYCOLYSIS_PATHWAY REACTOME_METABOLISM_OF_CARBOHYDRATES	Glycolysis and gluconeogenesis	ADPGK PFKFB4 TPI1 HK2 ALDOC	Lactate Dihydroxyacetone phosphate Hexose diphosphates Glucose 6-phosphate Pyruvate
Glutamate/ glutathione metabolism (growth phase)	KEGG_GLUTATHIONE_METABOLISM	Glutamate and glutathione metabolism	RRM2 SMS GSTM2	5-oxoproline glutamine N-acetylglutamine
Pentose phosphate pathway (NA)	KEGG_PENTOSE_PHOSPHATE_PATHWAY[a] KEGG_PENTOSE_AND_GLUCURONATE_ INTERCONVERSIONS[a]	Pentose metabolism and pentose pathway	H6PD TKT RPIA	Arabitol/xylitol Ribitol Arabonate/xylonate
Oxidative phosphorylation (NA)	KEGG_OXIDATIVE_PHOSPHORYLATION	NA	NDUFA7 COX6B1 ETFDH	NA
Glycosidases and deglycosylation (production phase)	GO_PROTEIN_DEGLYCOSYLATION	NA	FUCA1 HEXA NEU1	NA
Regulators of N-glycosylation (NA)	GO_REGULATION_OF_PROTEIN_ GLYCOSYLATION[a]	NA	TMEM59 IL15	NA

Table 1. Continued

NSD, nucleotide sugar donors; GPG, glycerophosphoglycerol ; GPC, glycerophosphocholine. Three orthogonal analyses (GSEA, TCGSA, and maSigPro) on the transcriptome and metabolome data were performed to identify key pathways that change over time. Top transcripts and metabolites based on maSigPro analysis are also shown (see also Data S15).

[a]Found significant in time course analysis, but not in the GSEA analysis.

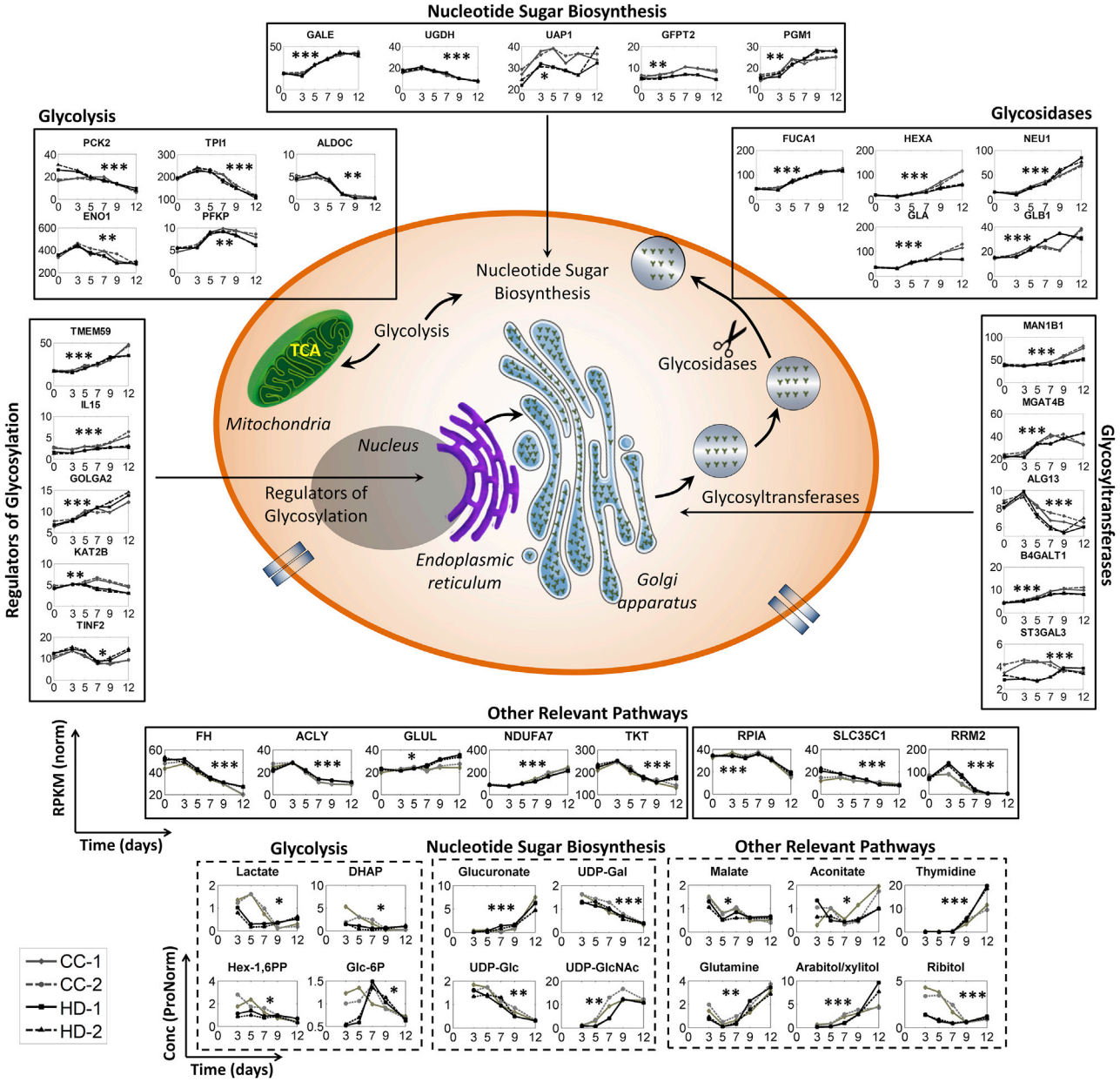

Figure 4. Transcriptional and Metabolic Factors that Can Potentially Affect N-Glycosylation Dynamics

Glycosylation dynamics can potentially be regulated via multiple ways as suggested by the time course and gene set enrichment analyses. Dynamics of top few transcripts (green blocks)/metabolites (red blocks) from each group that vary significantly with time are shown. A p value based on the time course analysis (maSigPro) is indicated by asterisks as follows: ***p <0.005, **0.005 > p > 0.01, *0.01 > p > 0.05.

fructose bisphosphate aldolase C (*ALDOC*), changed significantly over time (Data S12). Similarly, metabolites such as lactate, dihydroxyacetone phosphate, hexose diphosphates, and pyruvate were also found varying significantly with time (Data S13, Figures 4 and S4B).

Purine and Pyrimidine Metabolism

Purine and pyrimidine metabolism provides essential nucleotides during NSD biosynthesis such as cytidine triphosphate, guanosine triphosphate, and uridine triphosphate. Both these pathways are enriched in the growth phase (GSEA, Data S8B) and also show significant time dynamics in the time course analyses (Data S9 and S11). Several key enzymes involved in these pathways also vary significantly with time, such as ribose

phosphate pyrophosphokinase 1 (*PRPS1*), thymidylsynthatase (*TYMS*), uracil-DNA glycosylase (*UNG*), ribonucleoside-diphosphate reductase M2 (*RRM2*), and inosine-5′-monophosphate dehydrogenase 2 (*IMPDH2*). Several key metabolites also exhibit significant temporal dynamics, including thymidine, 2′-O-methylcytidine, and N1-methylinosine (Table 1).

TCA Cycle

The tricarboxylic citric acid (TCA) cycle is directly linked to glycolysis, glutamine, and purine and pyrimidine metabolic pathways (Figure S4B). Several gene sets related to the TCA cycle were enriched in the growth phase (GSEA, Data S8B). These gene sets also exhibited significant time dynamics (TCGSA, Data S9). The levels of several genes including those encoding for fumarate hydratase (*FH*), ATP citrate synthase (*ACLY*), NADP-dependent malic enzyme (*ME1*), and succinate dehydrogenase (*SDHC*) varied over time (maSigPro, Data S12). Interestingly, although the TCA cycle did not show up in TCMSA analysis, a few of its metabolites including aconitate, citrate, and malate were either up- or downregulated over time (Data S13).

Other Central Energy Metabolism Pathways

Other pathways linked to glycolysis and TCA cycle such as glutamine/glutamate metabolism (which serves as a precursor to N-acetylated NSD intermediates), pentose phosphate pathway (PPP), and oxidative phosphorylation showed significant time dynamics in their corresponding gene sets, transcripts, and metabolites (Table 1). For example, transketolase (*TKT*) and ribose-5-phosphate isomerase (*RPIA*) enzymes in the PPP decreased with time, whereas NADH dehydrogenase 1 alpha subcomplex 7 (*NDUFA7*) from oxidative phosphorylation increased with time (Figure 4, Data S12).

Glycosyltransferases

The concentration of glycosyltransferases can directly affect the reaction rates for each of the glycosylation steps. GSEA analysis suggested that gene sets containing glycosyltransferases were primarily enriched in the production phase (Data S8B). These gene sets also showed up significant in TCGSA analysis (Data S9). Several genes encoding for mannosidases and glycosyltransferases varied over time (Data S12, Figure 4). For example, 1,2-alpha mannosidases (*MAN1B1, MAN2A2, MAN2B1, MAN2B2,* and *MAN1A1*), N-acetylglucosamineyltransferases (*MGAT4B and MGAT1*), and beta-1,4-galactosyltransferase 1 (*B4GALT1*) increased over time (Figure S5). Other mannosidases (*MAN1C1*, *MAN2A1*, *MAN2C1*), fucosyltransferase (*FUT8*), and sialyltrasferases (*ST3GALT3* and *ST3GAL4*) showed marginal or no dynamics.

Glycosidases

Glycosidases catalyze cleavage of specific sugar moieties from the glycan structures on therapeutic proteins (and other host cell proteins). TCGSA strongly suggested that gene sets linked to glycan degradation vary significantly over time (Data S9), and GSEA analysis suggested that these gene sets are enriched in the production phase (Data S8B). Most of the glycosidase enzymes showed up in the maSigPro analysis including, fucosidase (*FUCA1*), galactosidases (*GLA, GLB1*), sialidases (*NEU1, NEU2, NEU3, NEU4*), and hexosidases (*HEXA, HEXB*) (Figure 4).

Other Regulators of Glycosylation

Apart from enzymes or gene sets that are directly linked to glycosylation, a gene set comprising regulators of glycosylation also showed up significant in GSEA and TCGSA analyses. The expression levels of most of the genes in this gene set increased over time (Figure 4, Data S12). These include transmembrane protein 59 (*TMEM59*), interleukin-15 (*IL15*) and golgin subfamily A member 2 (*GOLGA2*). For example, TMEM59 has been reported to be an inhibitor of galactosylation and sialylation (Ullrich et al., 2010). Temporal dynamics in transcript levels of *TMEM59* levels can affect the glycoforms produced.

In summary, functional analyses of time course omics data identified a number of enriched pathways and functional classes that can influence either the levels of substrates for NSD biosynthesis or the enzymes linked with the N-glycosylation process. These include genes and metabolites involved in glycolysis, TCA cycle, purine and pyrimidine biosynthesis, and amino sugar and NSD biosynthesis. Key genes and metabolites involved in these pathways that could be potential limiting factors for N-glycosylation are listed in Table 1 and Data S15. In the next section, a detailed analysis of the NSD biosynthetic pathway dynamics is performed.

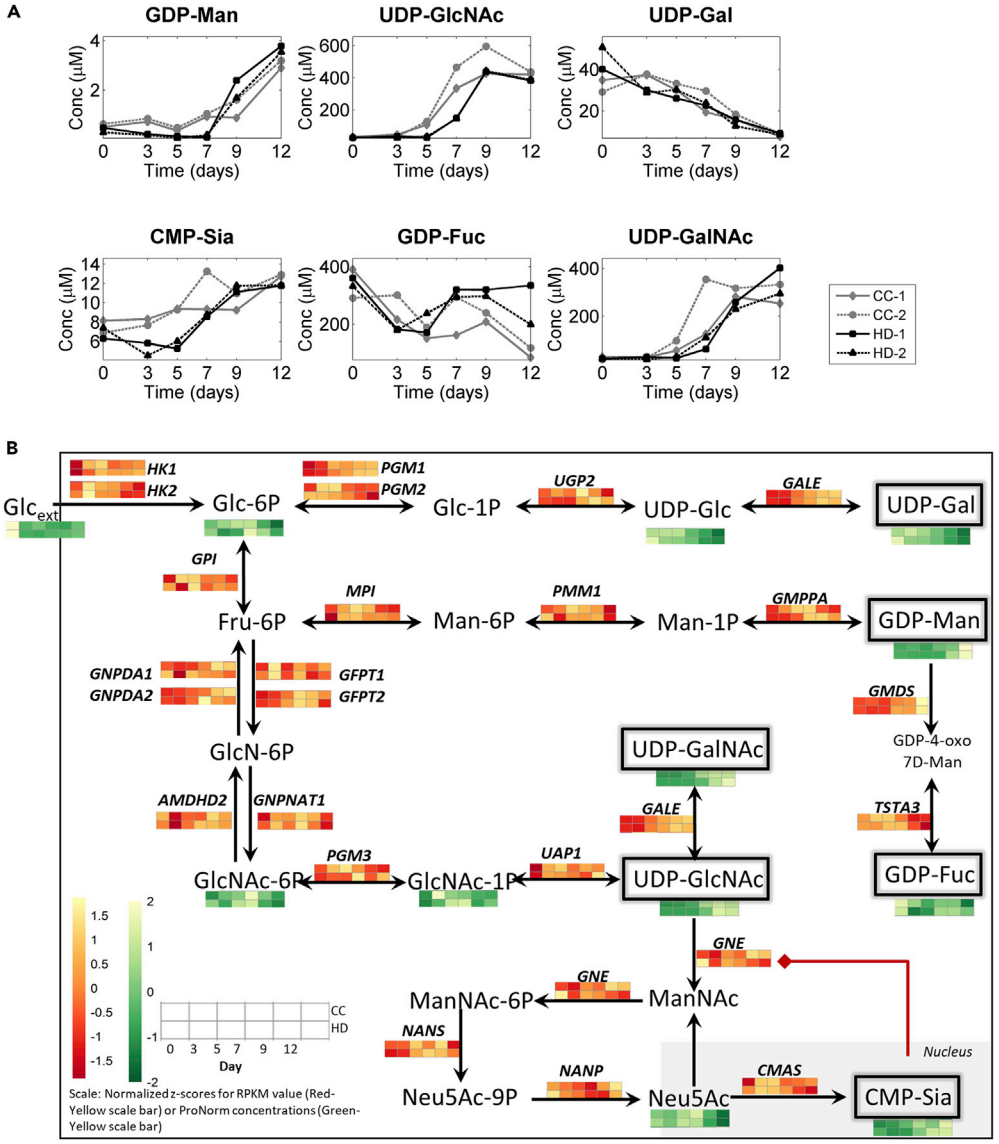

Figure 5. Time Dynamics of Nucleotide Sugar Donors and NSD Intermediates Partially Explains N-Glycosylation Dynamics Observed Experimentally

(A) Intracellular concentration of nucleotide sugar donors varies significantly over time for both processes.

(B) Overview of the temporal dynamics for the nucleotide sugar intermediates and transcripts that encode for enzymes involved in the nucleotide sugar biosynthetic pathways. A p value based on the time course analysis (maSigPro) for the RNA-seq and metabolomic data are available in Supplemental Information.

Analysis of Temporal Dynamics in Nucleotide Sugar Donor Biosynthetic Pathway Suggests Galactosylation and Sialylation Enzymatic Steps Might Be Substrate Limited

NSDs serve as substrates for the N-glycosylation process. Intracellular levels of NSDs were quantified from the cell pellet samples taken at multiple time points from the bioreactors for both fed-batch processes. The NSD concentrations varied over the course of fed-batch culture, and the dynamics for each NSD is conserved between the two fed-batch processes employed (Figure 5A). The dynamics in NSDs could be a result of temporal changes in the precursors from glycolysis and/or the enzymes and intermediate metabolites involved in the NSD biosynthetic pathways (Figure 5B). Time course transcriptome and metabolome data were used to probe biosynthetic pathway changes for each NSD, to identify the cause for temporal variation observed in the corresponding NSDs.

GDP-Mannose

Glucose is converted to G6P by hexokinase (*HK1* and *HK2*). G6P enters the NSD biosynthetic pathway and serves as a precursor to all the NSDs (Figure 5B). G6P exhibited significant time dynamics over the culture period (Data S13, Figure 5B). It is converted to F6P, which serves as the precursor for guanosine triphospho-mannose (GDP-Man) synthesis (Figure 5B). The intracellular concentration of GDP-Man increased during the course of the culture.

GDP-Fucose

Levels of guanosine triphospho-L-fucose (GDP-Fuc), which serves as the substrate for fucose addition to the glycan chain, for most part were relatively constant over the course of the culture for both the processes. GDP-Fuc is synthesized from GDP-Man in a two-step enzymatic process catalyzed by GDP-mannose 4,6 dehydratase (*GMDS*) and GDP-L-fucose synthase (encoded by the gene tissue-specific transplantation antigen P35B [*TSTA3*]) (Figure 5B). Marginal dynamics were observed in the transcript levels of the two enzymes, with GMDS going up with time and TSTA3 decreasing over time.

UDP-GlcNAc

Uridine diphospho-N-acetylglucosamine (UDP-GlcNAc) serves as the substrate for GlcNAc addition to the glycan chain. It is synthesized from G6P via intermediates including glucosamine-6-phosphate (GlcNAc6P) and glucosamine-1-phosphate (GlcNAc1P) (Figure 5B). UDP-GlcNAc increases significantly with time (~15-fold in CC; ~12-fold in HD), whereas no significant dynamics is observed for GlcNAc6P and GlcNAc1P (Data S13). The expression levels of the genes that encode the corresponding enzymes involved in the synthesis of GlcNAc1P also did not exhibit any significant time dynamics (Data S12). UDP-GlcNAc is also converted to Uridine diphospho-N-acetylgalactosamine (UDP-GalNAc) by UDP-glucose 4-epimerase, which is encoded by the gene *GALE*. UDP-GalNAc shows similar trends as UDP-GlcNAc despite significant increase in the expression level of *GALE* (Figure 5, Data S12).

UDP-Galactose

Uridine diphospho-galactose (UDP-Gal) serves as the substrate for galactose addition to the glycan chain. It is generally synthesized from G6P via a multi-step process (Figure 5B). G6P is initially converted to UDP-glucose (UDP-Glc), which is then converted to UDP-Gal by GALE. Transcript levels of enzymes involved in the UDP-Glc biosynthesis did not change significantly with time (Data S12), whereas the transcript levels of *GALE* were observed to increase with time. However, both UDP-Gal and UDP-Glc levels decreased significantly during the production phase (Figure 5A). As G6P levels decreased over time, the drop in UPD-Gal could be a direct result of decrease in G6P levels.

CMP-Sialic Acid

Cytidine monophospho-sialic acid (CMP-Sia) serves as the substrate for sialic acid addition to the glycan chain. Formation of CMP-Sia from UDP-GlcNAc is a multi-step process (Figure 5B). UDP-GlcNAc is converted to N-acetyl mannosamine (ManNAc) by the enzyme glucosamine (UDP-N-acetyl)-2-epimerase/N-acetylmannosamine kinase (GNE). ManNAc is converted to 5-acetyl neuraminic acid (Neu5Ac) by a series of enzymatic steps, which is then converted to CMP-Sia. CMP-Sia is known to strongly inhibit (with Hill coefficient = 4.1) the epimerase function of GNE, thus maintaining an autoregulation of CMP-Sia levels (Yardeni et al., 2011). The levels of CMP-Sia were in the lower concentration range, although a slight increase was observed over the course of the fed-batch processes (Figure 5A). Inhibition of the epimerase function of GNE by slightly higher concentrations of CMP-Sia might result in inhibition of UDP-GlcNAc conversion to downstream intermediates including Neu5Ac. This is observed to be the case as the Neu5Ac levels decreased over time, even though the levels of UDP-GlcNAc increased over time (Figure 5B).

Galactosylation and sialylation were observed to decrease over time (Figure 2B). Decrease in galactosylated species can now be explained by the decrease in the UDP-Gal levels over the course of the fed-batch culture. The decrease in sialylation can be explained by the decrease in galactosylated species over time. Relatively low availability of CMP-Sia does not help the drop in sialylation incurred due to the decrease in galactosylated species. With the help of the above-described understanding for the cause of the drop in the UDP-Gal levels and low levels of CMP-Sia, we next designed and performed experiments to overcome these bottlenecks in an attempt to increase and maintain a sustained level of galactosylation and sialylation in fed-batch cultures.

Temporal Rate Limitations in Galactosylation and Sialylation Can Be Mitigated by Supplementation of Corresponding NSD Biosynthetic Pathway Intermediates

To explore if the drop in the substrate (UDP-Gal) and/or cofactor (Mn^{2+}) levels of the enzyme that catalyzes galactosylation (B4galt1) is the root cause for the drop in the galactosylation of mAb glycoform produced, a pH-controlled fed-batch experiment was conducted in shake flasks with additional supplementation of galactose and/or Mn^{2+}. Galactose can be converted intracellularly to UDP-Gal by the action of enzymes encoded by *GALK* and *GALT*, the expression of which was observed to be relatively constant over the course of the fed-batch culture (Figure S6A). The shake flask experiment was performed using media used in the CC and HD bioreactor runs, with varying levels of Mn^{2+} (0.9 nM, 200 nM and 2,000 nM) or with combined supplementation of 5 g/L galactose and 2,000 nM Mn^{2+}. The additives were added to the culture on day 0. Manganese supplementation resulted in a decrease in cell growth in CC medium, whereas no such effect was observed in HD medium (Figure S6B). Time course glycan analysis suggested that although Mn^{2+} enhanced galactosylation, Mn^{2+} alone was insufficient to achieve high and sustained levels of galactosylation across the course of the culture (Figures 6A and S6). Interestingly, additional supplementation of galactose resulted in high and sustained levels of galactosylated species, which could be explained by the significantly higher UDP-Gal levels (Figure 6A). This established that maintaining higher levels of UDP-Gal and Mn^{2+} can help mitigate the drop in the galactosylation level over the course of a fed-batch culture.

Next, the effect of enhancing the substrate level for sialyltransferases, namely, CMP-Sia, on total sialylation was probed. As inferred in the previous section, it was hypothesized that low levels of CMP-Sia in fed-batch cultures could be due to the presence of active inhibitory feedback regulation of epimerase activity of GNE by CMP-Sia, limiting its own formation (autoregulation). The epimerase encoded by *GNE* converts UDP-GlcNAc to ManNAc. Supplementation of downstream metabolite of GNE, namely, ManNAc, can bypass this autoregulation by CMP-Sia resulting in higher levels of CMP-Sia, which has been previously demonstrated (Gu and Wang, 1998). However, supplementation of an upstream metabolite, namely, GlcNAc, should not result in increase in CMP-Sia. To test this, a fed-batch experiment with either no supplementation (control) or with supplementation of 20 mM ManNAc or GlcNAc was performed in pH-controlled shake flasks. For this experiment, HD medium supplemented with 2,000 nM Mn^{2+} and 5 g/L of galactose was used to ensure maximum possible levels of galactosylation. Day 3 and day 9 intracellular NSD and mAb glycan levels were measured for all conditions (Figures 6B and S7A). A 2-fold increase in sialylation was observed in case of ManNAc-supplemented media, but no such increase in sialylation was observed for GlcNAc-supplemented or control conditions (Figures 6B and S7B). In fact, a small drop in the sialylation was observed in the GlcNAc-supplemented condition when compared with the control condition, which could be attributed to a proportional drop in galactosylation observed (when compared with control) (Figures 6B and S7). The increase in the mAb sialylation in case of ManNAc supplementation could be explained by an ~24-fold increase in intracellular CMP-Sia levels compared to the control condition (Figure 6B). No significant change in CMP-Sia levels was observed in the GlcNAc-supplemented condition when compared to the control condition.

DISCUSSION

A fundamental challenge with therapeutic protein production using CHO fed-batch cultures is the heterogeneous glycoforms observed on the recombinant proteins at harvest. Glycoform heterogeneity at harvest is a cumulative effect of transient glycoform distribution integrated over the cell culture period. The transient glycoform distribution varies from one time point in culture to another. This heterogeneity in the transient glycoform distribution appears to be contributed by the changing glycosylation state of the cells with the progress of a fed-batch culture. In other words, the glycoforms produced at any given time point seem to change with time in a fed-batch culture (Figure S1C). Such temporal changes in glycosylation state could be a result of variation in multiple intrinsic factors including glycosyltransferase enzymes (Könitzer et al., 2015), NSDs (Hutter et al., 2017; Sha et al., 2016), by-products from central energy metabolism like ammonia (Gawlitzek et al., 2000), cofactors for glycosylation enzymes (Witsell et al., 1990), and host cell protein production (Park et al., 2017). To understand the underlying cause for dynamics of protein N-glycosylation across fed-batch cultures and identify key factors contributing to it, we employed a systems approach combining time course transcriptomics, metabolomics, and glycan analysis for a model CHO cell line producing a recombinant antibody in two variants of fed-batch culture (Figures 1 and 2).

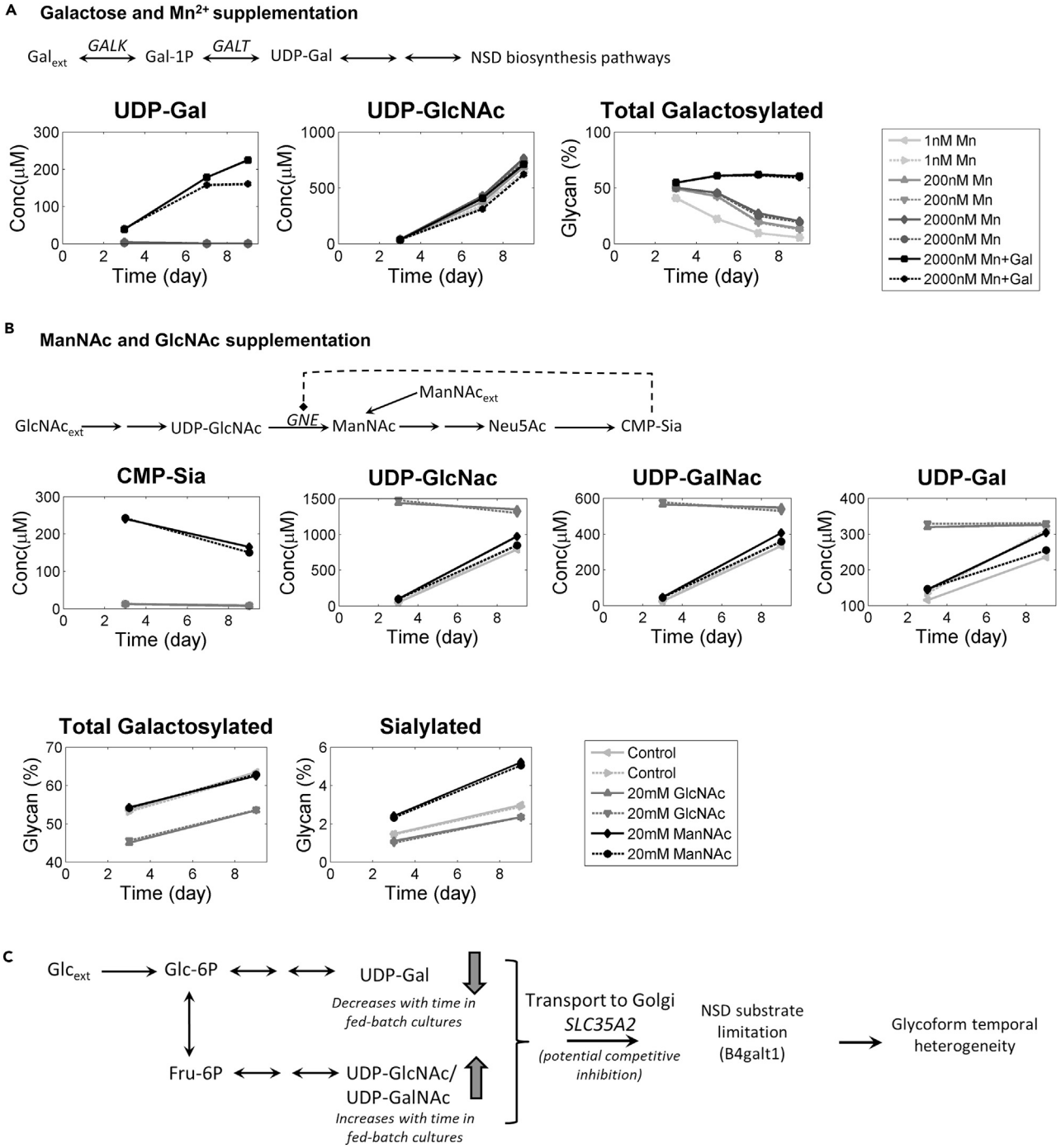

Figure 6. Media Supplementation Can Potentially Bypass the NSD Biosynthetic Pathway to Partially Mitigate Galactosylation and Sialylation Bottlenecks

(A) Supplementation of manganese to enhance B4galt1 activity alone is insufficient to reduce the bottleneck at galactosylation level, whereas galactose supplementation (5 g/L) leads to 25- to 50-fold increase in intracellular pool of UDP-Gal (left), resulting in sustained levels of galactosylation throughout the cell culture (right).

(B) Supplementation of 20 mM ManNAc bypasses the self-regulation on CMP-Sia biosynthesis (shown by dotted arrow) and leads to ~30-fold increase in intracellular concentrations of CMP-sialic acid (left), resulting in around 2-fold increase in sialylated species.

(C) Temporal variations in the intracellular concentrations of the NSD substrates and/or potential substrate competition for intra-Golgi transport due to shared transport protein might result in the temporal heterogeneity in glycoforms observed in fed-batch cultures.

Functional analysis of the omics data showed that a significant part of the time course variance in transcriptome, metabolome, and glycoform, at a global level, appeared to be a function of culture time and that a smaller fraction of the variance depended on the type of medium/process employed (Figure 3). Analysis of the glycoforms produced showed that one of the bottlenecks in the glycosylation pathway could be at the reaction step, which adds galactose to the extending glycan moiety (Figure S2). Employing statistical analysis approaches including GSEA, TCGSA, TCMSA, and maSigPro on transcriptome and metabolome data, it was observed that a number of glycosylation-affecting factors became more dynamically perturbed over the course of the culture, including metabolic pathways such as glycolysis, TCA cycle, pyrimidine/purine metabolism, nucleotide sugar synthesis, and other functional classes such as glycosidases (Table 1). The changes observed across the various metabolic pathways were due to changes at transcript or metabolite intermediate levels or in some cases due to both occurring simultaneously.

Glycosyltransferases are the primary factors that affect glycoform heterogeneity as they catalyze addition of sugar moieties to the extending glycan chain on a secretory protein (McDonald et al., 2016). The transcript levels of a number of glycosyltransferases were observed to change significantly over the culture time (Figure S5). However, these changes did not correlate with the glycoforms produced. For example, levels of galactosyltransferase (*B4GALT1*) increased with time, whereas galactosylation decreased with time. Similarly, 2-beta-N-acetylglucosaminyltransferase (*MGAT2*) decreased with time, whereas agalactosylated species increased with time. No significant dynamics was observed for alpha-(1,6)-fucosyltransferase (*FUT8*), whereas a marginal decrease in fucosylated species was observed over time. Sialylated species decreased over time in both processes, which could not be explained by the constant or marginal increased transcript levels of sialyltransferases (*ST3GALT3* and *ST3GAL4*). This suggested that the temporal variation of galactosylation and sialylation could be at the biochemical levels, i.e., enzyme cofactors and substrates (NSDs) (Hutter et al., 2017; Sha et al., 2016).

Glycolytic intermediates G6P and F6P are key carbon sources for all the NSD biosynthesis. Dynamics in the levels of glycolytic pathway activity can directly affect the NSD levels. Glycolytic pathway was observed to be enriched in growth phase with a number of glycolytic enzymes and glycolytic intermediates demonstrating time dynamics (Table 1, Data S12 and S13). Levels of G6P (and other upper glycolysis intermediates) decreased over time in the production phase of the cultures. Interestingly, the dynamics of intermediates in lower glycolytic pathway intermediates, namely 3-Phosphoglycerate (3PG) and Phophoenolpyruvate (PEP), increased over time. Glycolytic intermediates are known to have feedforward and feedback allosteric regulation on the upstream and downstream glycolysis enzymes imparting non-linear behavior to the flux and intermediate concentrations (Mulukutla et al., 2014, 2015). The dynamics observed in the levels of G6P and lower glycolysis intermediates could be an outcome of such non-linear allosteric regulations at play in addition to enzyme level changes.

Decrease in the levels of G6P in the production phase should result in a corresponding fall in the intracellular levels of the UDP-Gal, UDP-Man, and UDP-GlcNAc, which are NSDs produced directly from G6P through a chain of reactions. However, only UDP-Gal levels decreased with time, whereas UDP-GlcNAc and GDP-Man increased over time in the production phase of the cultures. This suggests that there are additional regulations within the UPD-GlcNAc and GDP-Man biosynthetic pathway segments. For example, increase in the UDP-GlcNAc levels could be due to increase in the levels of UDP-GlcNAc pyrophosphorylase encoded by the gene *UAP1*, an enzyme that catalyzes the conversion of GlcNAc-1P to UDP-GlcNAc (Figure 5B, Data S12). The increase in UDP-GlcNAc happens even though the levels of its direct precursor, GlcNAc-1P, decrease with time, which further strengthens the argument that increase in the levels of UAP1 could be at play here.

Levels of GDP-Fuc and CMP-Sia could be influenced by the levels of their precursors, GDP-Man and UDP-GlcNAc, respectively. Interestingly, the intracellular levels of GDP-Fuc remain relatively constant, although GDP-Man increases over the last 2 days of the culture. One explanation for this could be the decrease in the levels of fucose synthase enzyme (TSTA3) in the last 2 days of the culture. Similarly, even though UDP-GlcNAc levels increase significantly, only marginal increase in the levels of CMP-Sia were observed. This could be explained by the negative feedback regulation of an irreversible enzyme, GNE, in CMP-Sia biosynthetic pathway by itself. Supplementation of the intermediates downstream of the GNE, ManNAc, led to a significant increase in the CMP-Sia, further supporting the argument that auto feedback regulation could be at play. This regulation was also previously reported to be at play in CHO cells (Gu and Wang, 1998).

UDP-Gal, the NSD for the step of galactosylation, decreases with time for both the conditions (CC and HD) (Figure 5A). Assessing if the temporal changes in the NSD levels affect the glycoforms being produced, a clear correlation was observed between temporal decrease in protein galactosylation and intracellular levels of UDP-Gal. Another well-known factor that affects the level of galactosylation is manganese (Mn^{2+}), a cofactor that enhances B4galt1 activity (Witsell et al., 1990). Mn^{2+} concentration decreases with time even for the condition with higher Mn^{2+} (HD-1 and HD-2) (Figure S1D). Although manganese enhances galactosylation in a dose-dependent manner, supplementation of manganese alone fails to sustain high levels of galactosylation throughout the course of the culture (Figure 6A). Interestingly, in the presence of Mn^{2+}, supplementation of galactose to fed-batch cultures, which increased the intracellular UDP-Gal levels by 25- to 100-fold results in sustained levels of galactosylation for the entire cell culture period (Figure 6A). Galactose supplementation bypasses the glycolytic pathway for UDP-Gal biosynthesis, and galactose is converted to UPD-Gal by the Leloir pathway. The transcript levels of enzymes in the Leloir pathway, namely, GALK1, GALK2, GALT, and GALE, either increase or stay relatively constant across the fed-batch cultures (Figure S6A).

Furthermore, temporal reduction in galactosylation could also be partly due to the inhibition of UDP-Gal transport into *trans*-Golgi cisternae by increased levels of UDP-GalNAc and UDP-GlcNAc, observed in the late stages of the culture (Figure 5A). The NSD transport protein encoded by *SLC35A2* not only serves as a transporter for UDP-Gal, but is also reported to transport UDP-GalNAc (Song, 2013) and UDP-GlcNAc (Hadley et al., 2014). Therefore, each one of them can competitively inhibit transport of the other substrate. When cells were cultivated in GlcNAc-supplemented media, a significant increase in intracellular concentrations of UDP-Gal, UDP-GlcNAc, and UDP-GalNAc were observed (Figures 6B and S7A). This resulted in reduction in galactosylation when compared with control (Figures 6B and S7B). Interestingly, the ratio of UDP-Gal to UDP-GalNAc or UDP-GlcNAc was lower in the GlcNAc-treated condition when compared with control. These data further substantiate the hypothesis that increase in UDP-GalNAc and/or UDP-GlcNAc might negatively influence galactosylation (Figure 6C).

We also notice that UDP-Gal showed an increasing trend over time in a fed-batch culture upon galactose supplementation. Based on our hypothesis UDP-HexNAc (UDP-GlcNAc and UDP-GalNAc) competes with UDP-Gal for transport to Golgi. UDP-HexNAc was observed to increase over time intracellularly (Figure 6A). In the presence of such higher levels of UDP-HexNAc, and under sufficient availability of galactose, it is possible that to maintain the same flux of UDP-Gal through Golgi, the cytosolic UDP-Gal concentrations could increase.

Our study also shows that sialylation levels are very low and decrease with time. Galactose supplementation did not increase the peak levels of sialylation observed across the culture but helped prevent the drop in the sialylation observed during the production phase of the culture (Figure S6). This suggested that one reason behind temporal heterogeneity of sialylation is the heterogeneity in galactosylation levels. Another reason for low levels of sialylation could be the relatively lower levels of the corresponding NSD substrate (CMP-Sia). Evidently, supplementation of ManNAc increased the intracellular levels of CMP-Sia, which in turn enhanced the levels of sialylation. Interestingly, although ManNAc supplementation resulted in ~30-fold increase in the intracellular pool of CMP-Sia, the overall increase in sialylation was significantly low (from ~3% to ~5.5%). This suggests that, apart from the substrate limitations (availability of galactosylated species and CMP-Sia), other factors might be at play. These include, but are not limited to, low expression levels of sialyltransferases, reduced residence time for sialylation in *trans*-Golgi networks, and steric hindrance for sialyltransferases for glycan chain extension in case of mAbs (Dekkers et al., 2016).

Another potential factor that can influence temporal heterogeneity in glycan profile is the glycosidase activity. Glycosidases are prominently present in the extracellular matrix of the CHO fed-batch cultures for mAb production (Park et al., 2017). Addition of neuraminidases (glycosidases for sialic acid) results in reduced levels of sialylation in fed-batch cultures (Gramer et al., 1995). Functional analyses of the transcriptome data suggested that these glycosidases are significantly expressed and are enriched during production phase. We tested the effect of glycosidases present in the extracellular matrix by incubating the day 9 cell-free supernatants from cell cultures for 3 days at 36.5°C. When these samples were analyzed for changes in the glycan profile over the 3 days, only a slight reduction in the sialylation levels were observed (from ~2.9% to ~2.5%), whereas no significant differences were observed for other glycosylated species (data not shown). A possible reason why the effect was minimal is because the fed-batch cultures were maintained in the strict pH range of 6.9–7.2, whereas the optimum pH for most of these glycosidase activity

is within the pH range of 4–6 (Gramer and Goochee, 1993; Miyagi and Yamaguchi, 2012). Intracellularly, these glycosidases are known to localize primarily in lysosomes (Aronson and Kuranda, 1989; Miyagi and Yamaguchi, 2012) where pH is lower and suitable for their activity, such as participating in salvage pathways for misfolded proteins. Thus, despite exhibiting significant time dynamics, barring sialidases, other glycosidases might not directly influence the N-glycosylation dynamics in fed-batch cultures.

Functional analysis of the omics data also suggested genes and functional classes that might act as potential competitors for the common substrates (NSDs) and might affect the glycosylation dynamics. These include enzymes/genes that are involved in O-linked glycosylation, glycosaminoglycan, and glycosphingolipid synthesis. Although not completely understood, given the co-localization of some of these enzymes with those involved in N-glycosylation, these enzymes might compete for NSDs and even cofactors, thus influencing the dynamics. Similarly, the level and type of host cell glycoproteins secreted over the course of the culture might also affect the temporal changes in glycosylation of the mAb being produced. In addition, the specific productivity can potentially affect the residence time of the mAb within Golgi cisternae. Temporal changes in specific productivity can, therefore, result in the changes in the glycoforms produced with time. Additional work is needed to assess the role of these factors on glycosylation.

In conclusion, N-glycosylation is a complex dynamic process influenced by several pathways including NSD biosynthesis, glycolysis, and other processes that compete for enzymes or substrates. Systematic analysis of time course omics data identified the primary cause for glycosylation dynamics in fed-batch cultures as changes in the substrate availability. The holistic understanding of glycosylation network dynamics helped contrive strategies to overcome the bottlenecks toward reduction in the heterogeneity observed in fed-batch culture. Going forward, this understanding can be used to implement additional strategies to perform both process- and genetic-engineering-related modifications toward further reducing the glycoform heterogeneity observed in fed-batch cultures.

Limitations of the Study

In this study, in addition to identifying the cause for dynamics in N-glycosylation pathway activity and the glycoform produced, we made a number of observations that are intriguing but need to be probed further experimentally. First, we showed using one cell line with two distinct cell culture processes that glycoform dynamics are dominantly time dependent and less process dependent. Further experimentation with additional producing CHO cell lines across different lineages employing different fed-batch processes will be needed to be analyzed before fully establishing the generality of the above argument. Second, we identified other glycosylation-related pathways, including sphingolipid, glycerolipid, and aminoglycan biosynthesis, to be modulated in growth or production phases of the fed-batch processes. More experimentation is needed to probe the effect of competition for resources shared (nucleotide sugars, cofactors, and glycosylation enzymes) by these pathways along with protein glycosylation on the recombinant protein glycoform. Third, we observed that an increase in UPD-GlcNAc levels results in lower galactosylation. Experimentation is needed for identifying the mechanism at play.

METHODS

All methods can be found in the accompanying Transparent Methods supplemental file.

SUPPLEMENTAL INFORMATION

Supplemental Information includes Transparent Methods, 7 figures, and 15 data files and can be found with this article online at https://doi.org/10.1016/j.isci.2019.01.006.

ACKNOWLEDGMENTS

Authors thankfully acknowledge Gregory Hiller and Dana L. DiNino for their comments and suggestions during manuscript preparation.

AUTHOR CONTRIBUTIONS

M.S. and B.C.M. conceived and designed the experiments. M.S. performed the experiments. M.S. and S.D. analyzed the data. M.S., S.D., and B.C.M. wrote the manuscript. A.-H.A.C. and J.J.S. generated the experimental cell clone. A.-H.A.C., K.C., and J.K.M. performed glycan and nucleotide sugar analyses. A.-H.A.C., J.J.S.,A.A.C., J.K.M., R.W., D.A.L., B.F., and B.C.M. consulted on data analysis and edited the manuscript.

DECLARATION OF INTERESTS

The authors declare no conflict of interest.

Received: July 30, 2018
Revised: November 19, 2018
Accepted: January 3, 2019
Published: February 22, 2019

REFERENCES

Aronson, N.N., and Kuranda, M.J. (1989). Lysosomal degradation of Asn-linked glycoproteins. FASEB J. *3*, 2615–2622.

Berger, M., Kaup, M., and Blanchard, V. (2011). Protein glycosylation and its impact on biotechnology. In Genomics and Systems Biology of Mammalian Cell Culture (Springer), pp. 165–185.

Conesa, A., Nueda, M.J., Ferrer, A., and Talón, M. (2006). maSigPro: a method to identify significantly differential expression profiles in time-course microarray experiments. Bioinformatics *22*, 1096–1102.

Dekkers, G., Plomp, R., Koeleman, C.A.M., Visser, R., Von Horsten, H.H., Sandig, V., Rispens, T., Wuhrer, M., and Vidarsson, G. (2016). Multi-level glyco-engineering techniques to generate IgG with defined Fc-glycans. Sci. Rep. *6*, 1–12.

Eon-Duval, A., Broly, H., and Gleixner, R. (2012). Quality attributes of recombinant therapeutic proteins: an assessment of impact on safety and efficacy as part of a quality by design development approach. Biotechnol. Prog. *28*, 608–622.

Fan, Y., Jimenez Del Val, I., Müller, C., Wagtberg Sen, J., Rasmussen, S.K., Kontoravdi, C., Weilguny, D., and Andersen, M.R. (2015). Amino acid and glucose metabolism in fed-batch CHO cell culture affects antibody production and glycosylation. Biotechnol. Bioeng. *112*, 521–535.

Gawlitzek, M., Ryll, T., Lofgren, J., and Sliwkowski, M.B. (2000). Ammonium alters N-glycan structures of recombinant TNFR-IgG: degradative versus biosynthetic mechanisms. Biotechnol. Bioeng. *68*, 637–646.

Gramer, M.J., and Goochee, C.F. (1993). Glycosidase activities in Chinese hamster ovary cell lysate and cell culture supernatant. Biotechnol. Prog. *9*, 366–373.

Gramer, M.J., Goochee, C.F., Chock, V.Y., Brousseau, D.T., and Sliwkowski, M.B. (1995). Removal of sialic acid from a glycoprotein in CHO cell culture supernatant by action of an extracellular cho cell sialidase. Biotechnology (N. Y.) *13*, 692–698.

Gu, X., and Wang, D.I. (1998). Improvement of interferon-gamma sialylation in Chinese hamster ovary cell culture by feeding of N-acetylmannosamine. Biotechnol. Bioeng. *58*, 642–648.

Hackett, S.R., Zanotelli, V.R.T., Xu, W., Goya, J., Park, J.O., Perlman, D.H., Gibney, P.A., Botstein, D., Storey, J.D., and Rabinowitz, J.D. (2016). Systems-level analysis of mechanisms regulating yeast metabolic flux. Science *354*, aaf2786.

Hadley, B., Maggioni, A., Ashikov, A., Day, C.J., Haselhorst, T., and Tiralongo, J. (2014). Structure and function of nucleotide sugar transporters: current progress. Comput. Struct. Biotechnol. J. *10*, 23–32.

Hartley, F., Walker, T., Chung, V., and Morten, K. (2018). Mechanisms driving the lactate switch in Chinese hamster ovary cells. Biotechnol. Bioeng. *115*, 1890–1903.

Hejblum, B.P., Skinner, J., and Thiébaut, R. (2015). Time-course gene set analysis for longitudinal gene expression data. PLoS Comput. Biol. *11*, 1–21.

Hossler, P., Goh, L.-T., Lee, M.M., and Hu, W.-S. (2006). GlycoVis: Visualizing glycan distribution in the proteinN-glycosylation pathway in mammalian cells. Biotechnol. Bioeng. *95*, 946–960.

Hossler, P., Mulukutla, B.C., and Hu, W.-S.S. (2007). Systems analysis of N-glycan processing in mammalian cells. PLoS One *2*, e713.

Hsu, H.-H., Araki, M., Mochizuki, M., Hori, Y., Murata, M., Kahar, P., Yoshida, T., Hasunuma, T., and Kondo, A. (2017). A systematic approach to time-series metabolite profiling and RNA-seq analysis of Chinese hamster ovary cell culture. Sci. Rep. *7*, 43518.

Hutter, S., Villiger, T.K., Brühlmann, D., Stettler, M., Broly, H., Soos, M., and Gunawan, R. (2017). Glycosylation flux analysis reveals dynamic changes of intracellular glycosylation flux distribution in Chinese hamster ovary fed-batch cultures. Metab. Eng. *43*, 9–20.

Ivarsson, M., Villiger, T.K., Morbidelli, M., and Soos, M. (2014). Evaluating the impact of cell culture process parameters on monoclonal antibody N-glycosylation. J. Biotechnol. *188*, 88–96.

Jedrzejewski, P.M., del Val, I.J., Constantinou, A., Dell, A., Haslam, S.M., Polizzi, K.M., and Kontoravdi, C. (2014). Towards controlling the glycoform: a model framework linking extracellular metabolites to antibody glycosylation. Int. J. Mol. Sci. *15*, 4492–4522.

Jimenez del Val, I., Nagy, J.M., and Kontoravdi, C. (2011). A dynamic mathematical model for monoclonal antibody N-linked glycosylation and nucleotide sugar donor transport within a maturing Golgi apparatus. Biotechnol. Prog. *27*, 1730–1743.

Jiménez del Val, I., Constantinou, A., Dell, A., Haslam, S., Polizzi, K.M., and Kontoravdi, C. (2013). A quantitative and mechanistic model for monoclonal antibody glycosylation as a function of nutrient availability during cell culture. BMC Proc. *7*, O10.

Kaveh, O., Hengameh, A., Johannes, G., Murray, M.-Y., Legge, R.L., Jeno, S., and Budman, H.M. (2013). Novel dynamic model to predict the glycosylation pattern of monoclonal antibodies from extracellular cell culture conditions. IFAC *46* (31), 30–35.

Könitzer, J.D., Müller, M.M., Leparc, G., Pauers, M., Bechmann, J., Schulz, P., Schaub, J., Enenkel, B., Hildebrandt, T., Hampel, M., et al. (2015). A global RNA-seq-driven analysis of CHO host and production cell lines reveals distinct differential expression patterns of genes contributing to recombinant antibody glycosylation. Biotechnol. J. *10*, 1412–1423.

Krambeck, F.J., and Betenbaugh, M.J. (2005). A mathematical model of N-linked glycosylation. Biotechnol. Bioeng. *92*, 711–728.

Krambeck, F.J., Bennun, S.V., Narang, S., Choi, S., Yarema, K.J., and Betenbaugh, M.J. (2009). A mathematical model to derive N-glycan structures and cellular enzyme activities from mass spectrometric data. Glycobiology *19*, 1163–1175.

Lewis, N.E., Liu, X., Li, Y., Nagarajan, H., Yerganian, G., O'Brien, E., Bordbar, A., Roth, A.M., Rosenbloom, J., Bian, C., et al. (2013). Genomic landscapes of Chinese hamster ovary cell lines as revealed by the *Cricetulus griseus* draft genome. Nat. Biotechnol. *31*, 759–765.

Lin, N., Mascarenhas, J., Sealover, N.R., George, H.J., Brooks, J., Kayser, K.J., Gau, B., Yasa, I., Azadi, P., and Archer-Hartmann, S. (2015). Chinese hamster ovary (CHO) host cell engineering to increase sialylation of recombinant therapeutic proteins by modulating sialyltransferase expression. Biotechnol. Prog. *31*, 334–346.

Maverakis, E., Kim, K., Shimoda, M., Gershwin, M.E., Patel, F., Wilken, R., Raychaudhuri, S., Ruhaak, L.R., and Lebrilla, C.B. (2015). Glycans in the immune system and the altered glycan theory of autoimmunity: a critical review. J. Autoimmun. *57*, 1–13.

McDonald, A.G., Hayes, J.M., and Davey, G.P. (2016). Metabolic flux control in glycosylation. Curr. Opin. Struct. Biol. *40*, 97–103.

Miyagi, T., and Yamaguchi, K. (2012). Mammalian sialidases: physiological and pathological roles in cellular functions. Glycobiology *22*, 880–896.

Mulukutla, B.C., Gramer, M., and Hu, W.S. (2012). On metabolic shift to lactate consumption in fed-batch culture of mammalian cells. Metab. Eng. *14*, 138–149.

Mulukutla, B.C., Yongky, A., Daoutidis, P., and Hu, W.S. (2014). Bistability in glycolysis pathway as a physiological switch in energy metabolism. PLoS One *9*, e98756.

Mulukutla, B.C., Yongky, A., Grimm, S., Daoutidis, P., and Hu, W.S. (2015). Multiplicity of steady states in glycolysis and shift of metabolic state in cultured mammalian cells. PLoS One *10*, 1–20.

Mulukutla, B.C., Yongky, A., Le, T., Mashek, D.G., and Hu, W.S. (2016). Regulation of glucose metabolism – a perspective from cell bioprocessing. Trends Biotechnol. *34*, 638–651.

Nairn, A.V., York, W.S., Harris, K., Hall, E.M., Pierce, J.M., and Moremen, K.W. (2008). Regulation of glycan structures in animal tissues: transcript profiling of glycan-related genes. J. Biol. Chem. *283*, 17298–17313.

Niwa, R., and Satoh, M. (2015). The current status and prospects of antibody engineering for therapeutic use: focus on glycoengineering technology. J. Pharm. Sci. *104*, 930–941.

Opdam, S., Richelle, A., Kellman, B., Li, S., Zielinski, D.C., and Lewis, N.E. (2017). A Systematic evaluation of methods for tailoring genome-scale metabolic models. Cell Syst. *4*, 318–329.e6.

Park, J.H., Jin, J.H., Lim, M.S., An, H.J., Kim, J.W., and Lee, G.M. (2017). Proteomic analysis of host cell protein dynamics in the culture supernatants of antibody-producing CHO cells. Sci. Rep. *7*, 1–13.

Sathish, J.G., Sethu, S., Bielsky, M.-C., de Haan, L., French, N.S., Govindappa, K., Green, J., Griffiths, C.E.M., Holgate, S., Jones, D., et al. (2013). Challenges and approaches for the development of safer immunomodulatory biologics. Nat. Rev. Drug Discov. *12*, 306–324.

Sha, S., Agarabi, C., Brorson, K., Lee, D.-Y., and Yoon, S. (2016). N-glycosylation design and control of therapeutic monoclonal antibodies. Trends Biotechnol. *34*, 835–846.

Sha, S., Bhatia, H., and Yoon, S. (2018). An RNA-seq based transcriptomic investigation into the productivity and growth variants with Chinese hamster ovary cells. J. Biotechnol. *271*, 37–46.

Song, Z. (2013). Roles of the nucleotide sugar transporters (SLC35 family) in health and disease. Mol. Aspects Med. *34*, 590–600.

Sou, S.N., Sellick, C., Lee, K., Mason, A., Kyriakopoulos, S., Polizzi, K.M., and Kontoravdi, C. (2015). How does mild hypothermia affect monoclonal antibody glycosylation? Biotechnol. Bioeng. *112*, 1165–1176.

Subramanian, A., Tamayo, P., Mootha, V.K., Mukherjee, S., Ebert, B.L., Gillette, M.A., Paulovich, A., Pomeroy, S.L., Golub, T.R., Lander, E.S., et al. (2005). Gene set enrichment analysis: a knowledge-based approach for interpreting genome-wide expression profiles. Proc. Natl. Acad. Sci. U S A *102*, 15545–15550.

Ullrich, S., Münch, A., Neumann, S., Kremmer, E., Tatzelt, J., and Lichtenthaler, S.F. (2010). The novel membrane protein TMEM59 modulates complex glycosylation, cell surface expression, and secretion of the amyloid precursor protein. J. Biol. Chem. *285*, 20664–20674.

Villiger, T.K., Roulet, A., Perilleux, A., Stettler, M., Broly, H., Morbidelli, M., and Soos, M. (2016a). Controlling the time evolution of mAb N-linked glycosylation, Part I: Microbioreactor experiments. Biotechnol. Prog. *32*, 1123–1134.

Villiger, T.K., Scibona, E., Stettler, M., Broly, H., Morbidelli, M., and Soos, M. (2016b). Controlling the time evolution of mAb N-linked glycosylation - Part II: model-based predictions. Biotechnol. Prog. *32*, 1135–1148.

Witsell, D.L., Casey, C.E., and Neville, C. (1990). Divalent cation of galactosyltransferase in native activation mammary golgi vesicles. J. Biol. Chem. *265*, 15731–15737.

Yardeni, T., Choekyi, T., Jacobs, K., Ciccone, C., Patzel, K., Anikster, Y., Gahl, W.A., Kurochkina, N., and Huizing, M. (2011). Identification, tissue distribution, and molecular modeling of novel human isoforms of the key enzyme in sialic acid synthesis, UDP-GlcNAc 2-epimerase/ManNAc kinase. Biochemistry *50*, 8914–8925.

ISCI, Volume *12*

Supplemental Information

Dissecting N-Glycosylation Dynamics in Chinese Hamster Ovary Cells Fed-batch Cultures using Time Course Omics Analyses

Madhuresh Sumit, Sepideh Dolatshahi, An-Hsiang Adam Chu, Kaffa Cote, John J. Scarcelli, Jeffrey K. Marshall, Richard J. Cornell, Ron Weiss, Douglas A. Lauffenburger, Bhanu Chandra Mulukutla, and Bruno Figueroa Jr.

Supplemental Information

Supplemental Figures and Legends

Figure S1. Glycoforms attached to monoclonal antibodies produced in CHO fed-batch processes vary with time, and their relative levels could be affected by media components, Related to Figure 2.

A. Time course dynamics of extracellular metabolites and other cell/process variables are shown for CC and HD processes. For both processes, the cells in the culture behaved in similar fashion. B. Time dynamics of specific glycan structures attached to mAbs in cell culture. Various glycosylated species exhibit similar time dynamics despite process variation. C. Differential (instantaneous) time course profiles of major glycan species for the two processes, calculated by taking the differential of the cumulative glycans with respect to the titer produced (see Transparent methods). D. Time course metal ions and trace metal analysis of supernatant samples for both the processes. E. Glycan data from shake experiments under the two media conditions (CC and HD) with swapped manganese levels. Black lines represent data from HiPDOG (HD) process, while grey lines represent data from platform (CC) process.

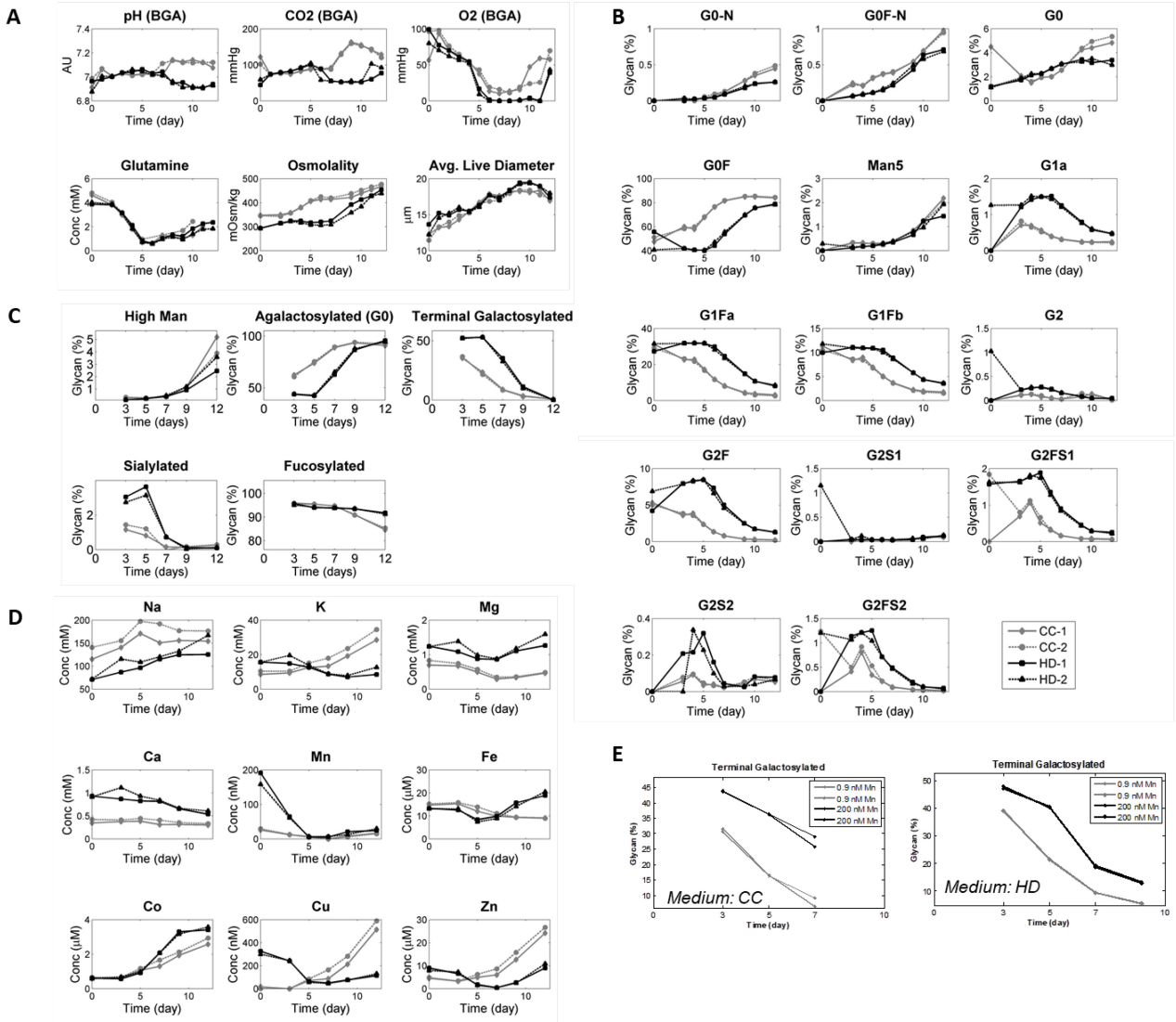

Figure S2. Galactosylation and sialylation steps serve as potential bottlenecks in the N-glycosylation process, Related to Figure 2.

Scatter plots between the fractions of consecutive major glycan species plotted on x-axis (i^{th} species) and y-axis ($i+1^{th}$ species). A. The data plot for G0-N *versus* high mannose species is primarily localized at the intersection of the two axes, suggesting that this step might not be rate limiting. B. The scatter plot of G0 species *versus* G0-N species is primarily localized on the y-axis of the graph, suggesting that GlcNAc addition might also not be rate limiting. C. When the total galactosylated species are plotted against G0 species, a negative correlation is observed, wherein G0 species increase while galactosylated species decrease with increasing time, suggesting that galactosylation might be rate limiting and the rate limitation increases over time. D. Scatter plot of sialylated species *versus* galactosylated species is primarily located near the x-axis of the graph suggesting a significant build-up of the precursors with time i.e. galactosylated species. The trends across days are depicted by lighter to darker shades of grey with increasing time. Arrows indicate time course direction.

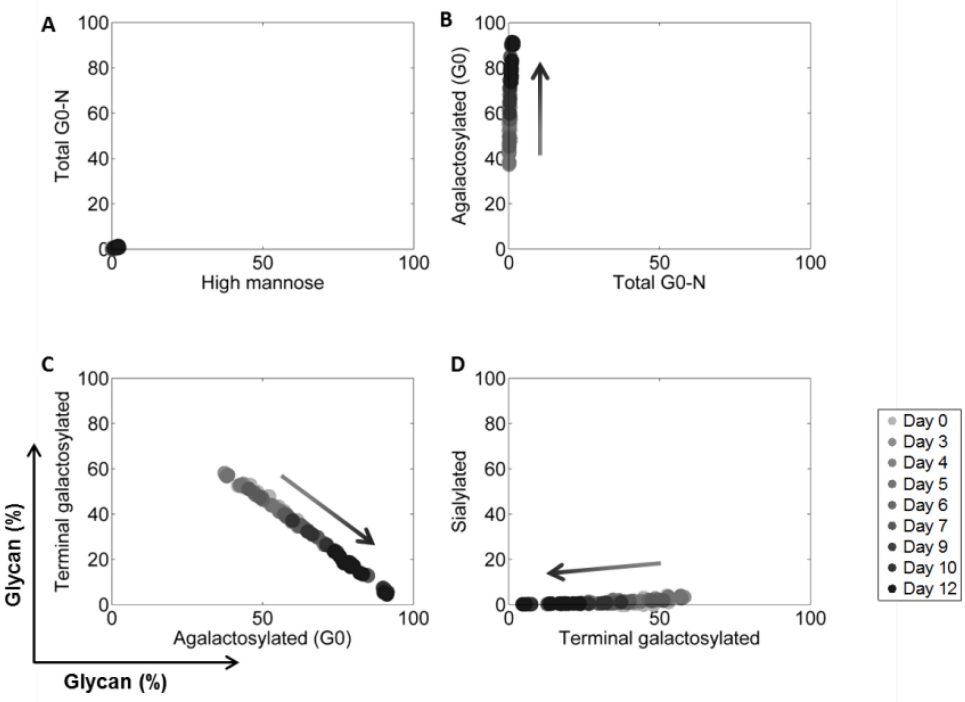

Figure S3. Gene set enrichment analysis of the time course transcriptome data for fed-batch process, Related to Figure 3.

Gene set enrichment analysis on pairwise comparisons of days in the growth phase (days 0, 3, 5) and production phase (days 7, 9 and 12). The bar lengths depict the number of day-by-day comparisons for which the gene set appears to be significantly enriched out of the nine possible day-by-day comparisons. A. A selection of gene sets that are enriched in growth phase. B. A selection of sets that are enriched in the production phase. For complete analysis, see Data S8a and Data S8b.

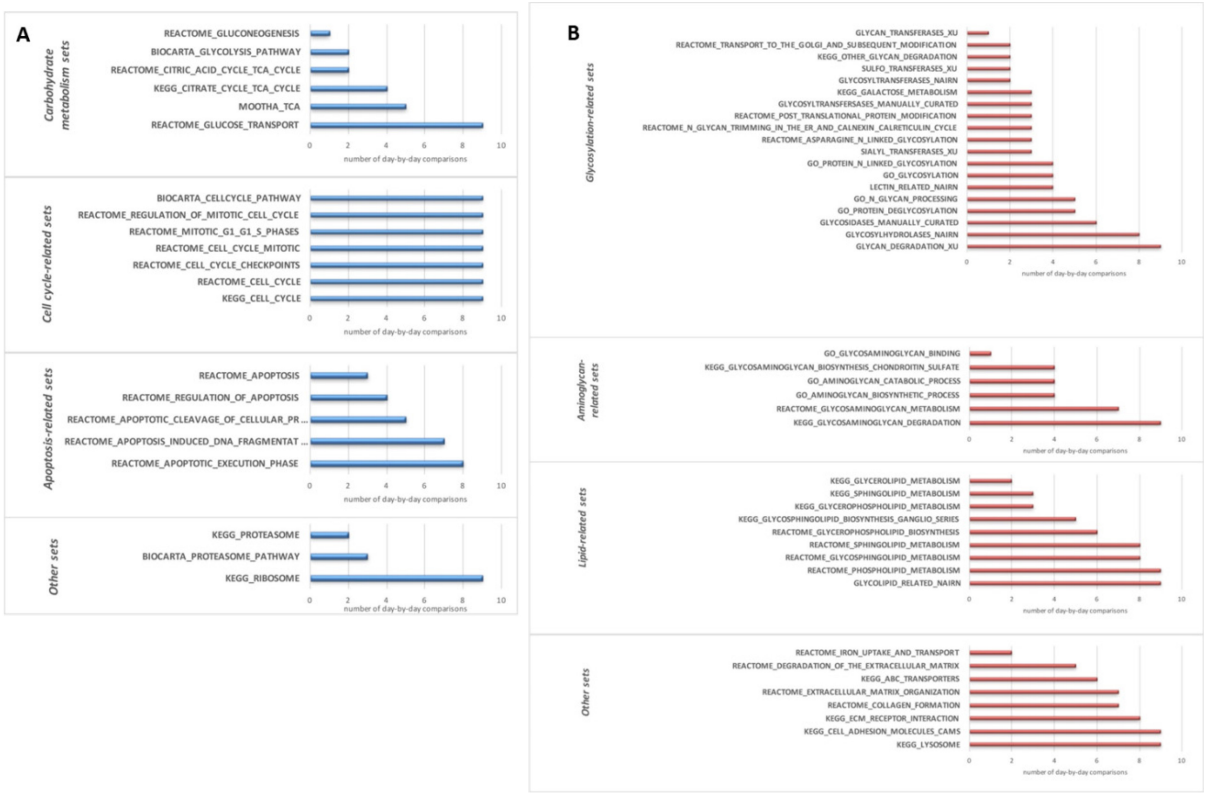

Figure S4. Shift in transcriptional and metabolic profile of CHO cells during cell culture is reflected in the central energy metabolism and related pathways linked to N-glycosylation, Related to Figure 4.

A. Specific glucose consumption and lactate production rates vary significantly over cell culture period for both the processes showing metabolic shift during the culture process. The switching of the ratio qLac/qGlc from positive to negative and back to positive suggests that cells undergo metabolic shifts in both the processes despite one being controlled for lactate (HD) while other not controlled (CD). B. Time dynamics of the metabolites and genes encoding for enzymes involved in central energy metabolism for the two processes. Throughout the cell culture, several enzymes and metabolites involved in central energy metabolism pathways show significant time variation. As these pathways provide precursors for the nucleotide sugar biosynthesis, the temporal variation can potentially affect the dynamics of NSD biosynthesis, thereby affecting in N-glycosylation dynamics.

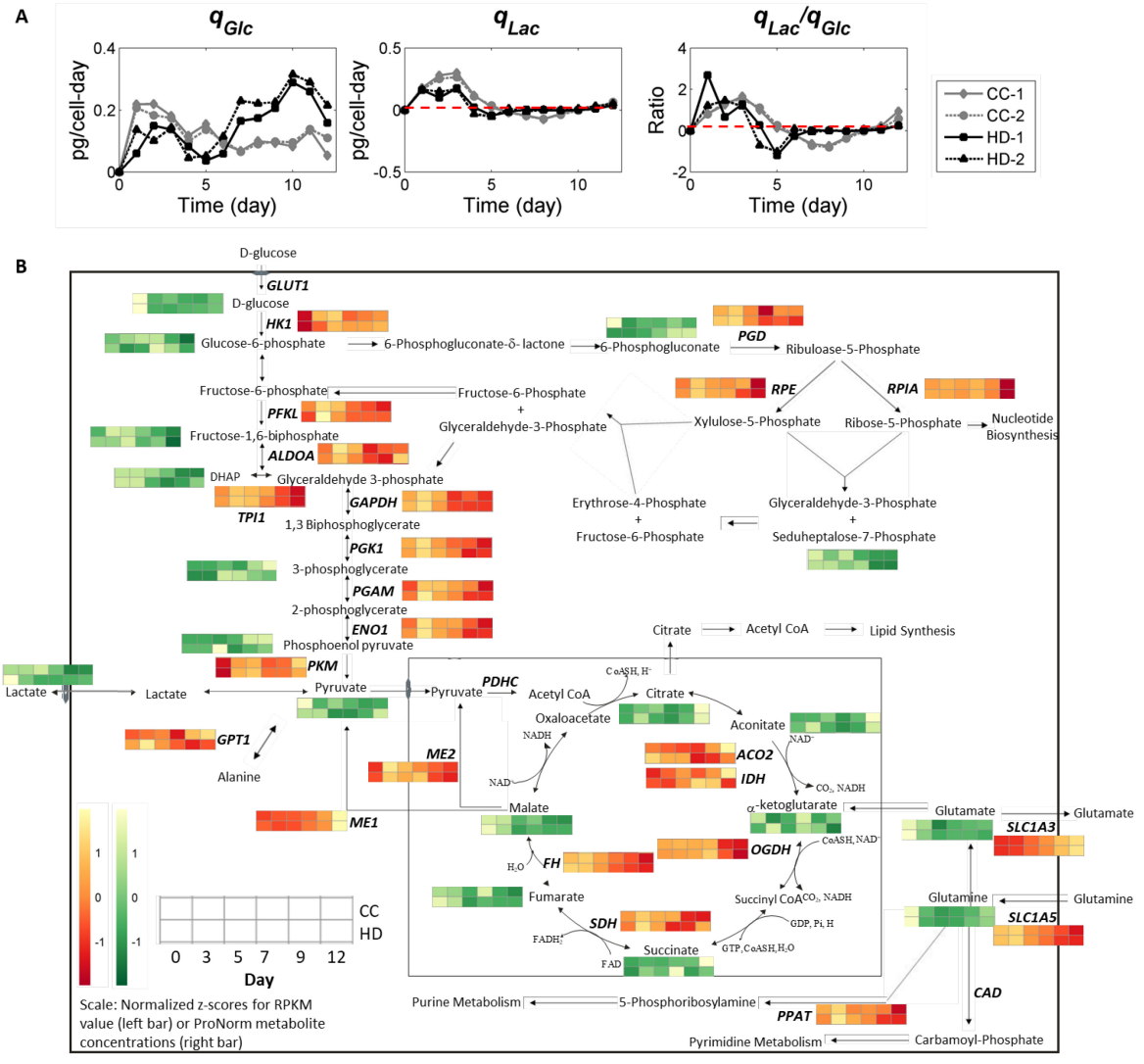

Figure S5. Transcript levels of several glycosylation related enzymes vary significantly with time, Related to Figure 5. Time dynamics of the transcripts of the enzymes directly involved in the N-glycosylation process and expressed in the CHO cell line used. Most of the transcripts wither increase over time or remain relatively constant, except *MGAT2*.

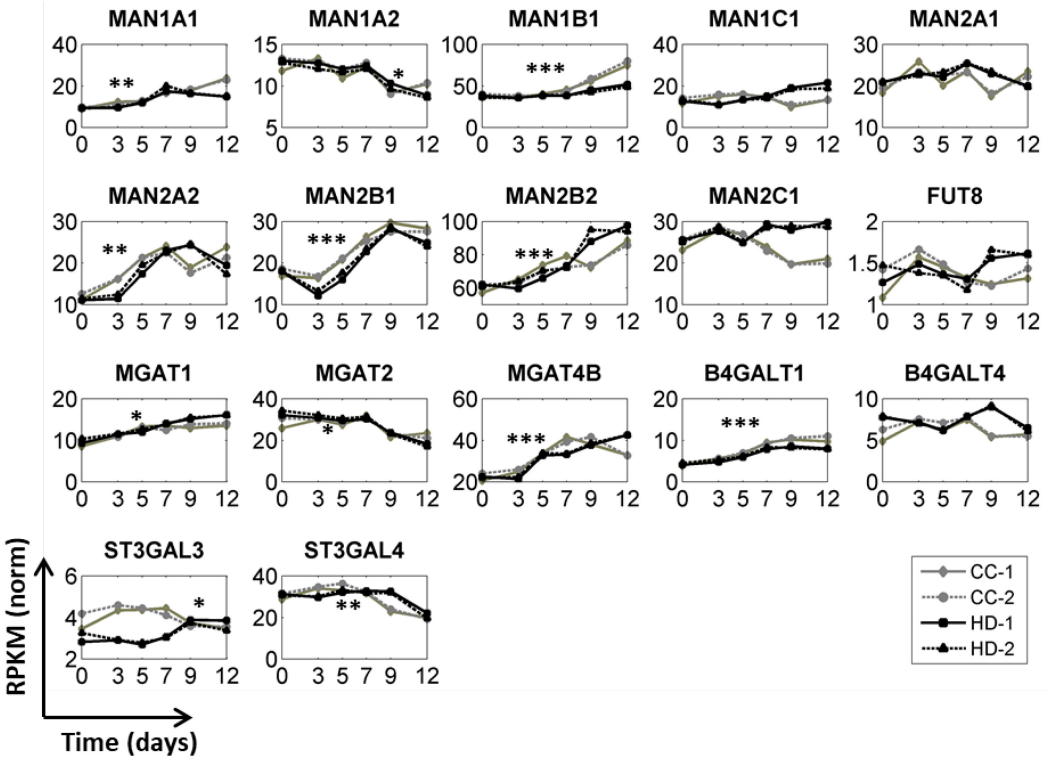

Figure S6. Galactose and not manganese overcomes the temporal heterogeneity in galactosylation, Related to Figure 6.

A. Time dynamics of transcripts of the enzymes involved in the Leloir pathway of UDP-Gal biosynthesis from external galactose supplementation. Both *GALK* and *GALT* remain relatively constant over the course of the fed-batch culture, while GALE increases over time. B. Supplementation of high concentration of manganese (2 uM) along with or without galactose (5g/L) affects cell growth in CC medium, while no significant difference is observed in HD medium. C, D. Glycan profiles of samples collected from cells cultured in fed-batch shake flasks with galactose and manganese supplementation. While manganese supplementation results in dose dependent increase in terminal galactosylated species, it alone is insufficient to sustain high levels of galactosylation in the later days in culture. Galactose supplementation results in sustained levels of galactosylation. The trends remain similar in both the media (CC and HD).

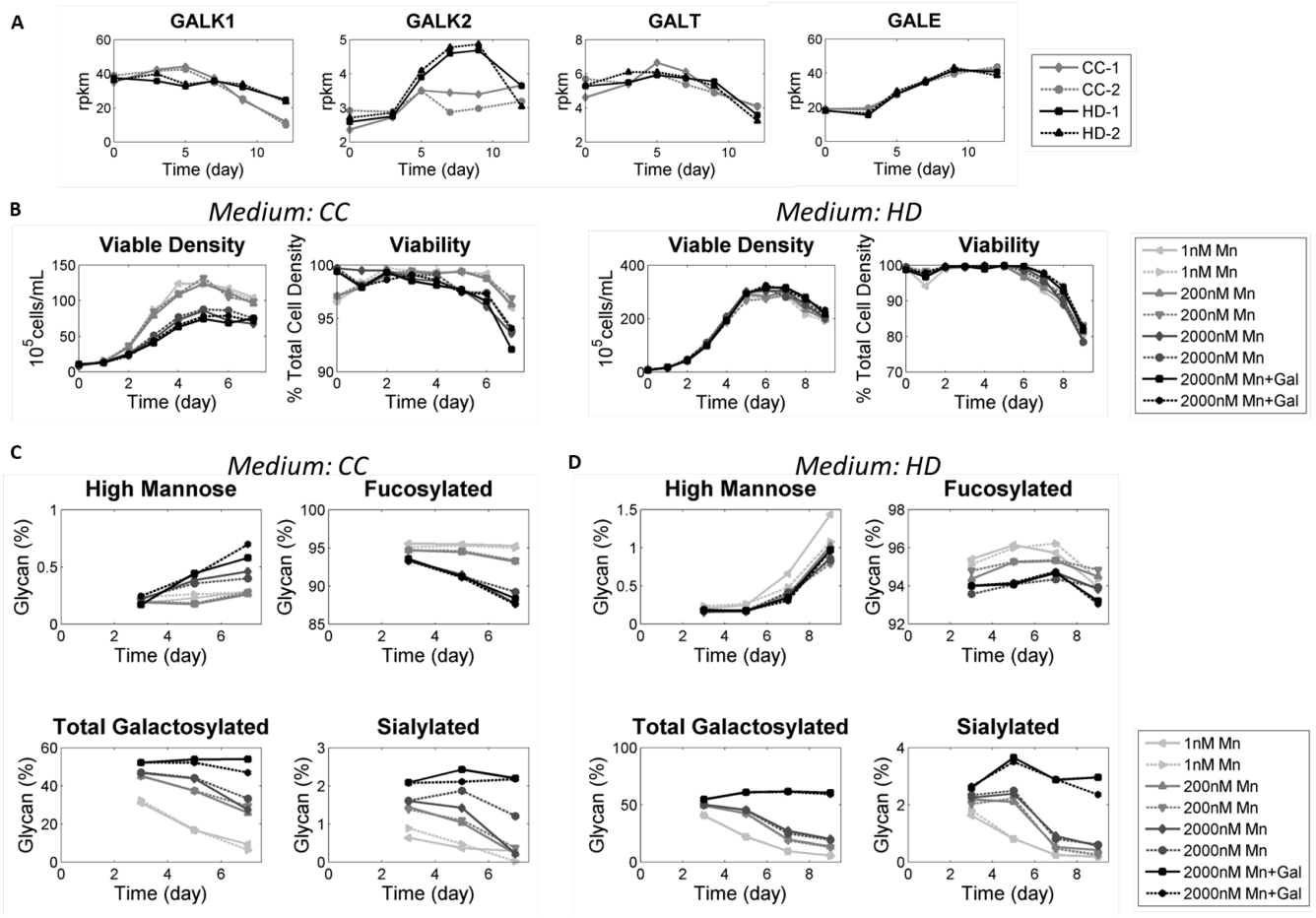

Figure S7. Bypassing CMP-Sia autoregulation by supplementing ManNAc significantly increases intra-cellular pool of CMP-Sia and marginally improves sialylation levels, Related to Figure 6.

A. Intracellular nucleotide sugar donor concentrations for the three conditions (a) control (b) 20 mM GlcNAc supplementation and (c) 20 mM ManNAc supplementation. All the three conditions were supplemented with 2000 nM Mn and 5g/L of Galactose. B. Glycan profiles for samples collected from cells cultured in fed-batch shake flasks with GlcNAc and ManNAc supplementation. Supplementation of ManNAc results around two-fold increase in sialylated species, while GlcNAc results in slightly lower sialylation levels. GlcNAc supplementation also affects the fractions of galactosylated, fucosylated and high mannose species.

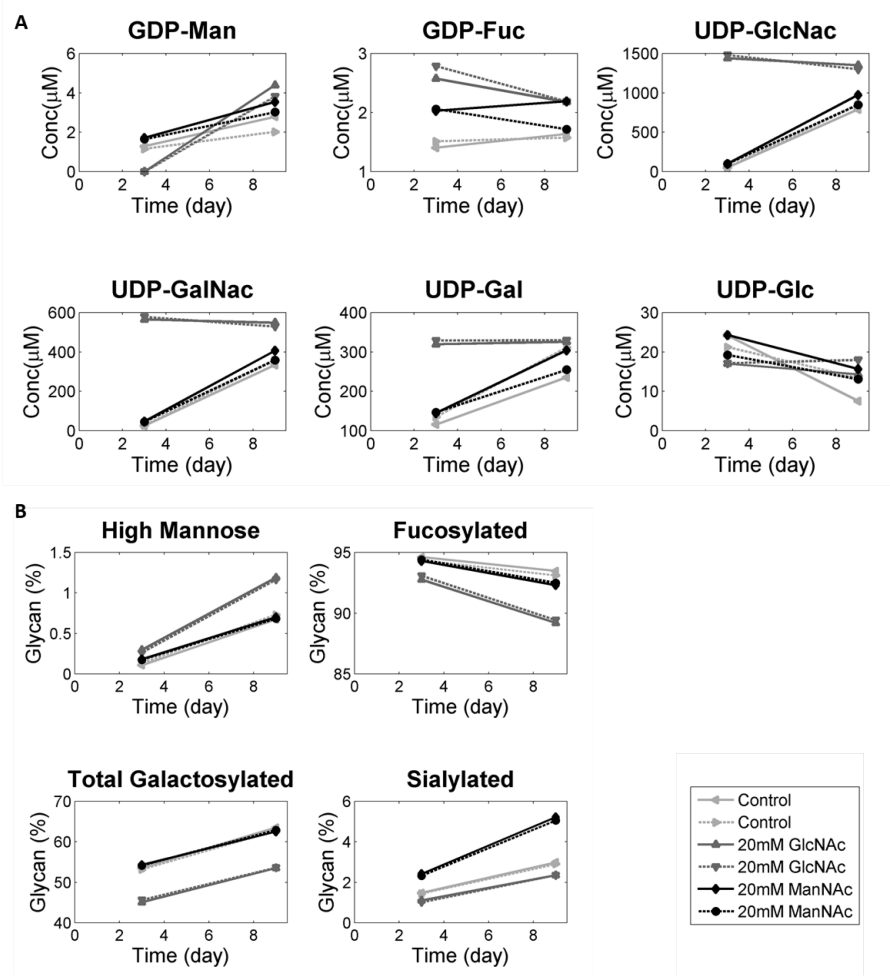

TRANSPARENT METHODS

KEY RESOURCES TABLE

REAGENT or RESOURCE	SOURCE	IDENTIFIER
Deposited Data		
Time course RNA-seq data	This paper	Data S3
Time course intracellular metabolic data	This paper	Data S4
Time course extracellular metabolic data	This paper	Data S5
Experimental Models: Cell Lines		
Hamster: CHO-K1 cell line	ATCC	CCL-61
Software and Algorithms		
edgeR package	(Robinson and Oshlack, 2010)	https://bioconductor.org/packages/release/bioc/html/edgeR.html
Principal Component Analysis	MathWorks Documentations	https://www.mathworks.com/help/stats/pca.html
pheatmap	CRAN-R	https://cran.r-project.org/web/packages/pheatmap/index.html
Gene Set Enrichment Analysis (GSEA)	(Subramanian et al., 2005)	https://software.broadinstitute.org/gsea/index.jsp
Time course gene set analysis (TCGSA)	(Hejblum et al., 2015)	https://cran.r-project.org/web/packages/TcGSA/index.html
maSigPro	(Conesa et al., 2006)	https://www.bioconductor.org/packages/release/bioc/html/maSigPro.html
Other		
Curate gene set list	This paper	Data S7
Curate metabolic set list	This paper	Data S10

CONTACT FOR REAGENT AND RESOURCE SHARING

Further information and requests for datasets and/or protocols may be directed to, and will be fulfilled by the Lead Contact Bhanu Chandra Mulukutla (BhanuChandra.Mulukutla@pfizer.com).

EXPERIMENTAL MODEL AND SUBJECT DETAILS

Cell line development

The CHO-K1 cell line (ATCC) was adapted to serum free, suspension growth. Approximately 10 million cells were transfected with a vector expressing both the heavy and light chain genes for the mAb, as well

as a puromycin resistance selectable marker by electroporation. After 24 hours, cells were spun down and re-suspended in media containing 10 µg/mL of puromycin to select for cells with stable vector integration. After addition of selective agent, cells were plated in static 48-well plates at an approximate density of 2000 cells per well. After 3 weeks, wells were screened for mAb titer, and high expressing wells were pooled together, and expanded to shake flasks. After one passage, the cell pool was FACS cloned (Aria II, Becton Dickinson) to one cell per well using previously described methods (Zhang et al., 2015). Subsequent scale up and octet titer screening were performed on clones to select 30 clones for shake flask cultures. The clone with the highest octet titer was chosen to perform the bioreactor and shake flask experiments. Cells were grown in shake flasks with CD-CHO media supplemented with 6mM Glutamine and 10 µg/L of Puromycin (Mirrus, Fisher Scientific).

Fed-batch processes description

Two fed-batch processes were employed as part of this study. These included a platform process (CC-1 and CC-2) that used a modified CD-CHO commercial media as a basal production medium and, a HiPDOG process (HD-1 and HD-2) that used an internally developed high nutrient production medium and employed a HiPDOG (high end pH control of glucose) strategy (Gagnon et al., 2011). The HiPDOG strategy helps restrict lactate production in fed-batch cultures without compromising on the proliferative capability of cells (Gagnon et al., 2011). For both processes, internally developed distinct feed medium and feeding strategies were used. In the CC process, glucose was maintained above 1.5 g/L throughout the process. In the HD process, glucose concentration was kept low by intermittent addition of feed medium containing glucose at the high end of pH dead-band of the process when the HiPDOG strategy was operational (i.e. from day 2-5) and above 1.5 g/L during the post-HiPDOG phase.

Fed-batch bioreactor experiments

Duplicate bioreactor vessels were inoculated at 1E6 viable cells/mL for two different production media viz. platform (CC-1 and CC-2) and HiPDOG (HD-1 and HD-2). The bioreactors were maintained at a pH of 7.05±0.05 in case of CC-1 and CC-2, and at 7.025±0.025 in case of HD-1 and HD-2. Day 6 onwards, the pH for both the conditions was set at 7.05±0.15. Dissolved oxygen was controlled at 40% of air saturation by micro-bubble sparging of a mixture of CO_2/air and O_2. Temperature was controlled at 36.5°C. Several metabolites and biophysical characteristics such as glucose, lactate, K^+, Na^+, Ca^{++}, NH_4^+, glutamate, glutamine, viable cell density, osmolality, and average live cell diameter were determined daily using a NOVA Flex BioProfile Analyzer (Nova Biomedical, Waltham, MA). Offline pH, O_2 and CO_2 measurements were taken daily using a 248 CIBA-Corning blood gas analyzer (Bayer AG, Leverhusen, Germany). The cell culture were sampled on specific days (Day 0, 3, 5, 7, 9 and 12) for cell pellets and supernatant to perform several time course analyses including transcriptomic (RNA-seq) and metabolomics analyses, glycan analysis, nucleotide-sugar analysis as well as for titer measurements. Titers were analyzed using a protein A HPLC (model 1100 HPLC, Agilent Technologies, Inc., Santa Clara, CA, protein A column model 2-1001-00, Applied Biosystems, Foster City, CA).

Fed-batch shake flask experiments

Duplicate shake flasks were inoculated at 1E6 viable cells/mL in either CC medium or in HD medium with added 7 g/L glucose. 6 mM Glutamine was supplemented in the media before inoculation. The flasks were maintained at 36.5°C and 5% CO2 and the shaker speed was set at 140 rpm. pH adjustment to 7.1 was performed daily for each of the flasks using a base solution ($NaHCO_3$ and $KHCO_3$ solution). Appropriate volume of 50% glucose was added so that the glucose in the medium is maintained at a level higher than 1.5 g/L.

Mathematical definition used in the manuscript

a. IVCC based specific productivity (q_P) for *i*th time-point measurement is given by: $q_P = \frac{Titer_i}{IVCC_i}$, where $IVCC_i = IVCC_{i-1} + \frac{(VCD_i + VCD_{i-1})}{2} * (time_i - time_{i-1})$.

b. Specific glucose consumption (q_{Glc}) for *i*th time-point is given by: $q_{Glc} = \frac{rGlc_{consumption}}{0.5*(VCD_i + VCD_{i-1})}$, where, $rGlc_{consumption} = \frac{Glucose_i - Glucose_{i-1} + Glucose\ from\ nutrient\ feed}{time_i - time_{i-1}}$.

c. Specific lactate production (q_{Lac}) for *i*th time-point is given by: $q_{Lac} = \frac{Lactate_i - Lactate_{i-1}}{0.5*(VCD_i + VCD_{i-1})*(time_i - time_{i-1})}$.

METHOD DETAILS

Protein-A purification materials and methods

Protein-A purification materials: 1:1 mixture of Milli-Q water, Acetonitrile (ACN-Omnisolve), trifluoroacetic acid (TFA-Thermo Scientific), PNGaseF (N-glycanase-Prozyme), 5x sodium phosphate buffer (Prozyme), sodium cyanoborohydride (Fluka), DMSO (Fluka), 2-aminobenzamide (Fluka), glacial acetic acid (Sigma), octanal (Sigma-Aldrich), Protein A resin (GE MabSelect), HILIC column: Xbridge Amide 3.5 um, 4.6x150 mm (Waters). Sodium phosphate (J.T. Baker), Acetonitrile (Omnisolve), 1M Tetrabutylammonium acetate (Sigma-Aldrich), Methanol (EMD-Millipore), Phenomenex Aeris PEPTIDE, 1.7 µm, 150 x 2.1 mm, Agilent Zorbax 300SB-CN 5 µm, 4.6 x 250 mm, Amicon 10KMWCO filter (EMD-Millipore). mAb select

Protein-A purification methods: Protein-A resin was washed and added to a 1:1 mixture of sample:water. After incubating at room temperature for 45 minutes in a rocker, the supernatant was removed and the pellets were added to a 96-well plate. The wells of the plate were washed three times with water. To elute the glycans, 6 µL of 0.5 M Tris base pH 10.8 was added to the receiver tray and 250 µL of 50 mM glycine 25 mM sodium chloride pH 3.00 was added to the filter plate. Concentration was determined using the Nano-Drop.

Glycan analysis

Glycan release from mAb: Approximately 100 µg of protein A purified mAb at a volume not exceeding 100 µL was combined with 6 µL of 5x phosphate buffer and 2 µL (4µL if reaction volume >50µL) of PNGaseF and incubated for approximately 16 hours at 37ºC. 10µL of 2-AB derivitization solution (0.35M 2-aminobenzamide/ 1M sodium cyanoborohydride dissolved in a 30/70% acetic acid/DMSO) was added to each sample and incubated for 2 hours at 65ºC. Sample volume was brought to 100µL with water and combined with 600 µL of octanal (Chu et al., 2018). Samples were vortexed and the bottom fraction was filtered through a 0.1 µm spin filter and diluted to 30/70% sample/ACN prior to injection.

Chromatograhy: Mobile phase A (A): 0.05% (v/v) TFA in ACN. Mobile phase B (B): 0.05% (v/v) TFA in Water. HILIC column: Xbridge Amide 3.5 um, 4.6x150 mm (Waters). Temperature: 45ºC. Sample Temperature: 5ºC. System: Waters Alliance. Flow rate: 1mL/min. Fluorescence detector Excitation: 330 nm, Emission: 420 nm. Run time: 60 minutes. Injection volume: 30µL. Gradient: 0-5 min 28% B, 5-42 min 28-42%B,42-43 min 42-90%B, 43-44 min 90%B, 44-45 min 90-28%B, 45-60 min 28%B. For each run sample peaks were identified by retention time comparison to a mass spectrometry characterized reference material.

Intracellular nucleotide sugar analysis

Cellular extraction: 5-10 E6 cells washed in cold PBS and snap frozen were thawed on ice and mixed with 100µL of cold 50:50 ACN:water. Samples were vortexed and centrifuged at 13000g. Supernatant samples were dried in a speedVac, reconstituted in 100 µL of water, and filtered through an Amicon 10kMWCO filter prior to injection.

Chromatography: Mobile Phase A (A): 100 mM Sodium phosphate pH 5.1, 8 mM tetrabutylammonium acetate. Mobile Phase B (B): 30% methanol, 70%A. Two columns were combined in tandem 1 (pump side): ThermoFisher Scientific Accucore Vanquish C18+, 1.5 µm, 100 x 2.1 mm, 2: Agilent Zorbax 300SB-CN 5 µm, 4.6 x 250 mm. Temperature: 15°C. Sample Temperature: 5°C. System: Waters Acquity UPLC H-Class Bio. Flow rate: 0.2 mL/min. UV 260 nm detection. Run Time: 140 minutes. Injection Volume: 5 µL. Gradient: 0-40 min 1%B, 40-90 min 1-50%B, 90-110 min 50%B, 110-111 min 50-1%B, 111-140 min 1%B. Sample peaks were identified by comparison to a reference standard with known amounts of nucleotides and nucleotide sugars bracketed throughout the run.

Differential glycan calculations

The cumulative glycan profile obtained experimentally was transformed into differential glycan data using two-point time derivative with respect to the titer. Mathematically, if Gi,tk is the cumulative value for i^{th} glycan structure on day 'tk', and Ttk is the titer produced until that day, then the differential glycan values can be calculated by using the following relation:

$$g_{j,t_m} = \frac{G_{j,t_m} \times T_{t_m} - G_{j,t_{m-1}} \times T_{m-1}}{\Delta T_{t_m}}$$

Metal ions and trace metal analysis

5 mL of supernatant samples were collected for days 0, 3, 5, 7, 9 and 12 for each of the bioreactors (CC-1, CC2, HD-1 and HD-2). The samples were analyzed using inductively coupled plasma (ICP) mass spectrometry method to determine concentrations of several metal ions known to affect CHO cell metabolism (Figure S1D). For a few of the metal ions, such as sodium, potassium and calcium, the concentrations were also determined using the NovaFlex instrument, confirming that the ICP analysis and NovaFlex measurements were consistent.

RNA-seq analysis

Cell culture from bioreactors were sampled and spun down at 1000 rpm into cells pellets of about 10E6 viable cells and dissolved in Trizol (ThermoFisher Scientific, Waltham, MA) and was flash frozen in dry ice/ethanol bath. The dissolved and frozen cells were sent to Beijing Genomics Institute (BGI, Hong Kong) for RNA isolation, library preparation and sequencing analysis. Samples were run on Illumina HiSeq 2000. RNA-Seq data were mapped to CHO genome using subjunc aligner program from subread-1.4.6 package. The alignment bam files were compared against the gene annotation GFF file, and raw counts for each gene were generated using the featureCounts tool from subread. The raw counts were normalized using TMM method (Robinson and Oshlack, 2010) and the reads per kilobase per million (RPKM) values for each gene was calculated using the edgeR package (https://bioconductor.org/packages/release/bioc/html/edgeR.html).

Intracellular and extracellular metabolomic analyses

Cell pellets (10E6 cells) flash frozen in dry ice/ethanol and supernatant (1 mL) from each bioreactor for each sampling day were sent to Metabolon (Metabolon Inc, Morrisville, NC) for metabolomics analyses. Proteins were removed by methanol precipitation and the metabolites were recovered by vigorous shaking and centrifugation. The extracted samples were run for reverse phase (RP)/UPLC-MS/MS (Ultrahigh Performance Liquid Chromatography-Tandem Mass Spectroscopy) with negative ion mode ESI and for

HILIC/UPLC-MS/MS with negative mode ESI. Raw data was extracted, peak-identified and QC processed using Metabolon's hardware and software. The raw ion count data was normalized against the extracted proteins quantified using Bradford assay.

QUANTIFICATION AND STATISTICAL ANALYSIS

Principal Component Analysis (PCA) and Cluster Analysis

After the addition of a value of 1 to RPKM expression values, and performing quantile normalization, principal component analysis was performed in MATLAB on the log2 transformed gene expression data. Each sample was considered an observation and each gene was considered a variable.

Pair-wise cluster analysis was performed for the time point samples for their transcriptome data, intracellular and extracellular metabolite data as well as glycan data. Spearman correlation was used to cluster the samples using the pheatmap package in R. The variance of each gene over time was calculated and the top 10% varying genes were selected for the analysis. This was done to remove the less-varying genes that might not carry the temporal information.

PCA loadings for the transcriptome, extracellular metabolites, intracellular metabolites, as well as for glycosylation related gene set is provided in Data S14. Factors with large loadings indicate that their variations would contribute the most to the particular principal components.

Gene Set Enrichment Analysis (GSEA)

A pair-wise permutation of all the samples within each process (CC or HD) were analyzed using GSEA method to identify pathways that are enriched in either growth phase or in production phase (Data S8b). A score was calculated based on how many times a particular gene-set showed up significant (p-value < 0.05) in CC or HD or both processes for the pairwise permutations.

Preprocessing: To minimize the noise from the low expressing genes, a value of 1 was added to the RPKM gene expression values. Subsequently, quantile normalization was performed so that all samples have a similar expression distribution and to alleviate the inter-sample biases. A manually curated gene set was compiled by combining three curated canonical pathways databases including BioCarta, KEGG, and Reactome, taken from the Broad Institute's Molecular Signatures database v6.0 (MSigDB) (Liberzon et al., 2015). Additional glycan-related gene sets taken from Gene Ontology databases as well as four gene sets comprised of the genes in nucleotide sugar synthesis were added to the combined list. The resulting gene set list is provided as Data S7.

GSEA analysis: Gene set enrichment analysis (GSEA) method was adapted to analyze the time course RNA-seq data from a published source (Subramanian et al., 2005). A two-step analysis was performed: (i) pair-wise comparison of days from distinct phases of cell culture, i.e. growth phase (days 0, 3, 5) and production phase (days 7, 9 and 12), to identify sets that are over-represented in each phase (Data S8a), and (ii) find how many times a gene set was enriched in either of the growth or production phases (Data S8b). For each of these nine comparisons between growth and production phases, GSEA was run using the desktop version with the following settings: Gene sets database: number of permutations: 1000 and permutation type: Gene_set. Since the number of samples in each comparison was 4 (2 per days compared), gene set permutation was performed as recommended by GSEA guidelines as follows. Enrichment statistic: Weighted; Metric for ranking genes: log2_Ratio_of_Classes; Max size: exclude larger sets: 500; Min size: exclude smaller sets: 10 and FDR cut-off of 0.05 was used to select the enriched gene sets that are significant. The outcomes of these set of analyses are the gene sets where its member genes are either enriched or lowered in one phase over another in a coordinated manner (see Data S8b).

Time course gene set analysis (TCGSA)

An extension of gene set analysis for longitudinal data sets (time course data) is available as TCGSA package in R (Hejblum et al., 2015). TCGSA considers a time series data as a single vector measurement and utilizes generalized linear (and/or non-linear) models to compare the two vectors. Thus, in our study, TCGSA was used to analyze gene sets that had time dynamics in the entirety of the cell culture period. This was done by comparing the time series measurement (Day 0 through Day 12) with the basal (Day 0) levels to gain insight into which functional groups were significantly perturbed over the course of cell culture time period. In this method, a gene set is said to be significant if its expression is not stable over time once the variability for genes and biological conditions are accounted for. The genes within a gene sets are modeled with mixed models that includes variables for gene, biological condition, time, intercepts in gene sets as well as random effects and variabilities. The mixed models fit the gene expression profiles to linear polynomials or cubic polynomials or natural cubic splines. For the sake of simplicity, we used the linear polynomial method for our analysis. The null hypothesis that the genes in a gene set are stable over time is compared with alternate hypothesis that the genes may vary significantly over time. A likelihood ratio is calculated for each of the gene sets based on these two hypotheses and a p-value for the significance of the variation of a gene set over time is computed. Multiple testing hypothesis was accounted for by using Bejamini-Yekutieli procedure to control the false discovery rate. A corresponding adjusted p-value or q-value was computed for each of the gene sets under different biological conditions such as media (CC vs HD) and different phases such growth phase (Day 0 – Day 7) vs production phase (Day 7 – Day 12). The RPKM data was pre-processed similarly as described in the previous section for the GSEA analysis.

Time course metabolic set analysis (TCMSA)

An adaptation of TCGSA (described in the previous sub-section), using the same software package was implemented on the time course intracellular metabolomic data set. A curated list of metabolic functional sets was used (see Data S10).

Time course significance analysis of individual transcripts and metabolites using maSigPro

maSigPro is a regression based approach that identifies genes for which there are significant gene expression profile differences between experimental groups in a time course microarray and RNA-seq experiments. An R package available for maSigPro analysis was used to analyze the transcriptomic data (Conesa et al., 2006). maSigPro package was used on quantile normalized rna-seq data and metabolome data to calculate false discovery rate (FDR) normalized p-values for each gene/metabolite that show differential expression over time. Additionally, same approach was implemented on the protein normalized intracellular metabolomic data to identify key metabolites that exhibit significant time profiles during the cell culture.

Statistical analysis and significance

For the statistical tests employed in the manuscript, including two-tailed unpaired t-test, GSEA, TCGSA and maSigPro, statistical significance is defined as $p < 0.05$. A gene or metabolic set (in case of TCGSA/TCMSA) or a gene/enzyme (in case of maSigPro analysis) 'exhibiting significant time dynamics' means that the adjusted p-value is < 0.05 and statistically, they show significant perturbations or changes over the cell culture period.

DATA AND SOFTWARE AVAILABILITY

The time course transcriptomic data, intracellular and extracellular metabolomic data and data generated from the time course omics analyses (functional analyses) are provided in Data S1-S15.

Supplemental References

Chu, A.H.A., Saati, A.E., Scarcelli, J.J., Cornell, R.J., and Porter, T.J. (2018). Reactivity-driven cleanup of 2-Aminobenzamide derivatized oligosaccharides. Anal. Biochem. *546*, 23–27.

Conesa, A., Nueda, M.J., Ferrer, A., and Talón, M. (2006). maSigPro: A method to identify significantly differential expression profiles in time-course microarray experiments. Bioinformatics *22*, 1096–1102.

Gagnon, M., Hiller, G., Luan, Y.T., Kittredge, A., Defelice, J., and Drapeau, D. (2011). High-End pH-controlled delivery of glucose effectively suppresses lactate accumulation in CHO Fed-batch cultures. Biotechnol. Bioeng. *108*, 1328–1337.

Hejblum, B.P., Skinner, J., and Thiébaut, R. (2015). Time-Course Gene Set Analysis for Longitudinal Gene Expression Data. PLoS Comput. Biol. *11*, 1–21.

Liberzon, A., Birger, C., Thorvaldsdóttir, H., Ghandi, M., Mesirov, J.P., and Tamayo, P. (2015). The Molecular Signatures Database Hallmark Gene Set Collection. Cell Syst. *1*, 417–425.

Robinson, M.D., and Oshlack, A. (2010). A scaling normalization method for differential expression analysis of RNA-seq data. Genome Biol. *11*.

Subramanian, A., Tamayo, P., Mootha, V.K., Mukherjee, S., Ebert, B.L., Gillette, M.A., Paulovich, A., Pomeroy, S.L., Golub, T.R., Lander, E.S., et al. (2005). Gene set enrichment analysis: a knowledge-based approach for interpreting genome-wide expression profiles. Proc. Natl. Acad. Sci. U. S. A. *102*, 15545–15550.

Zhang, L., Inniss, M.C., Han, S., Moffat, M., Jones, H., Zhang, B., Cox, W.L., Rance, J.R., and Young, R.J. (2015). Recombinase-mediated cassette exchange (RMCE) for monoclonal antibody expression in the commercially relevant CHOK1SV cell line. Biotechnol. Prog. *31*, 1645–1656.